Article

Neuron

Cortical Neurogenesis Requires Bcl6-Mediated Transcriptional Repression of Multiple Self-Renewal-Promoting Extrinsic Pathways

Graphical Abstract

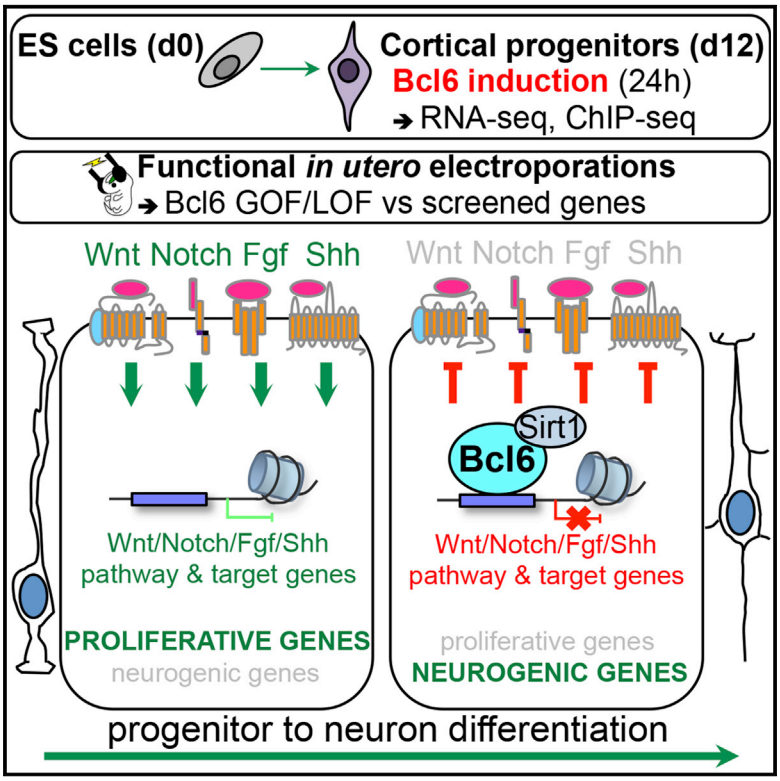

Authors

Jerome Bonnefont, Luca Tiberi, Jelle van den Ameele, ..., François Guillemot, Stein Aerts, Pierre Vanderhaeghen

Correspondence

pierre.vanderhaeghen@kuleuven.vib.be

In Brief

Bonnefont et al. show that Bcl6 promotes neurogenesis by directly repressing genes belonging to the major signaling pathways promoting cortical progenitor self-renewal. These data indicate that a single cell-intrinsic factor represses multiple extrinsic signaling pathways to ensure irreversible neurogenic commitment.

Highlights

- Bcl6 ensures robust neurogenesis by repressing major extrinsic self-renewal pathways
- Bcl6 inhibits the Notch, Wnt, SHH, and FGF signaling pathways at multiple levels
- Bcl6 represses transcription through Sirt1 recruitment and histone deacetylation

Bonnefont et al., 2019, Neuron *103*, 1096–1108
September 25, 2019
https://doi.org/10.1016/j.neuron.2019.06.027

CellPress

CellPress

Neuron
Article

Cortical Neurogenesis Requires Bcl6-Mediated Transcriptional Repression of Multiple Self-Renewal-Promoting Extrinsic Pathways

Jerome Bonnefont,[1,2] Luca Tiberi,[1] Jelle van den Ameele,[1] Delphine Potier,[2] Zachary B. Gaber,[3] Xionghui Lin,[1] Angéline Bilheu,[1] Adèle Herpoel,[1] Fausto D. Velez Bravo,[1,2] François Guillemot,[3] Stein Aerts,[2] and Pierre Vanderhaeghen[1,2,4,5,6,*]

[1]Université Libre de Bruxelles (ULB), Institut de Recherches en Biologie Humaine et Moléculaire (IRIBHM), and ULB Neuroscience Institute (UNI), 1070 Brussels, Belgium
[2]VIB-KU Leuven Center for Brain & Disease Research, 3000 Leuven, Belgium
[3]The Francis Crick Institute, London NW1 1AT, UK
[4]Department of Neurosciences, Leuven Brain Institute, KU Leuven, 3000 Leuven, Belgium
[5]Welbio, Université Libre de Bruxelles (ULB), 1070 Brussels, Belgium
[6]Lead Contact
*Correspondence: pierre.vanderhaeghen@kuleuven.vib.be
https://doi.org/10.1016/j.neuron.2019.06.027

SUMMARY

During neurogenesis, progenitors switch from self-renewal to differentiation through the interplay of intrinsic and extrinsic cues, but how these are integrated remains poorly understood. Here, we combine whole-genome transcriptional and epigenetic analyses with *in vivo* functional studies to demonstrate that Bcl6, a transcriptional repressor previously reported to promote cortical neurogenesis, acts as a driver of the neurogenic transition through direct silencing of a selective repertoire of genes belonging to multiple extrinsic pathways promoting self-renewal, most strikingly the Wnt pathway. At the molecular level, Bcl6 represses its targets through Sirt1 recruitment followed by histone deacetylation. Our data identify a molecular logic by which a single cell-intrinsic factor represses multiple extrinsic pathways that favor self-renewal, thereby ensuring robustness of neuronal fate transition.

INTRODUCTION

During neural development, the generation of the appropriate type and number of differentiated neurons and glial cells is controlled by a complex interplay between extrinsic and intrinsic cues acting on neural progenitors, thus regulating the balance between differentiation and self-renewal (Martynoga et al., 2012; Rossi et al., 2017; Tiberi et al., 2012b).

In the developing cortex, radial glial cells are the main progenitors that will differentiate into specific postmitotic neuron populations, directly or through various classes of intermediate progenitors (Götz and Huttner, 2005; Kriegstein and Alvarez-Buylla, 2009). Proneural factors act on these progenitors as the main intrinsic drivers of neurogenesis (Guillemot and Hassan, 2017; Guillemot et al., 2006), through cross-repression with the Notch pathway, which promotes self-renewal, and by directly inducing various classes of genes involved in neuronal differentiation. Key features of the Notch signaling pathway, such as lateral inhibition and oscillatory behavior, contribute in a major way to the irreversible commitment of differentiating cells toward neuronal fate (Kageyama et al., 2008). Moreover, many classes of extrinsic morphogen cues, including Wnt ligands, Sonic Hedgehog (SHH), and fibroblast growth factors (FGFs) can act on cortical progenitors to promote expansion and self-renewal and thereby effectively block neurogenesis (Chenn and Walsh, 2002; Kang et al., 2009; Lien et al., 2006; Rash et al., 2011; Wang et al., 2016).

Intriguingly, it has long been proposed that postmitotic cells undergoing neuronal differentiation become insulated from extrinsic signaling (Edlund and Jessell, 1999). Whether and how responsiveness to extrinsic cues is negatively modulated to allow neuronal commitment remains essentially unclear. Delamination of the progenitors away from the ventricular zone could contribute to this process, as some of these cues are secreted in the embryonic cerebrospinal fluid and are thought to act through the apical processes or cilia of the radial glial cells (Lehtinen et al., 2011). However, several cues, most strikingly Wnts, are also present in the cortical tissue (Harrison-Uy and Pleasure, 2012), where they can act on progenitors to block differentiation.

Moreover, the signaling components of these various pathways, as well as some key downstream targets, are often partially overlapping. For instance, cross-talk of the Notch and Wnt pathways (Hayward et al., 2008), or Notch and FGFs (Rash et al., 2011), has been documented during embryonic development and, despite the relatively simple intracellular regulation of the Wnt/β-catenin pathway, many of its components are used by other pathways or participate in distinct cellular activities. For instance, the deletion of *Gsk3a/b*, a major intracellular component of the β-catenin destruction complex, increases the proliferation of radial glial cells at the expense of their differentiation by altering not only Wnt but also Notch and FGF signaling

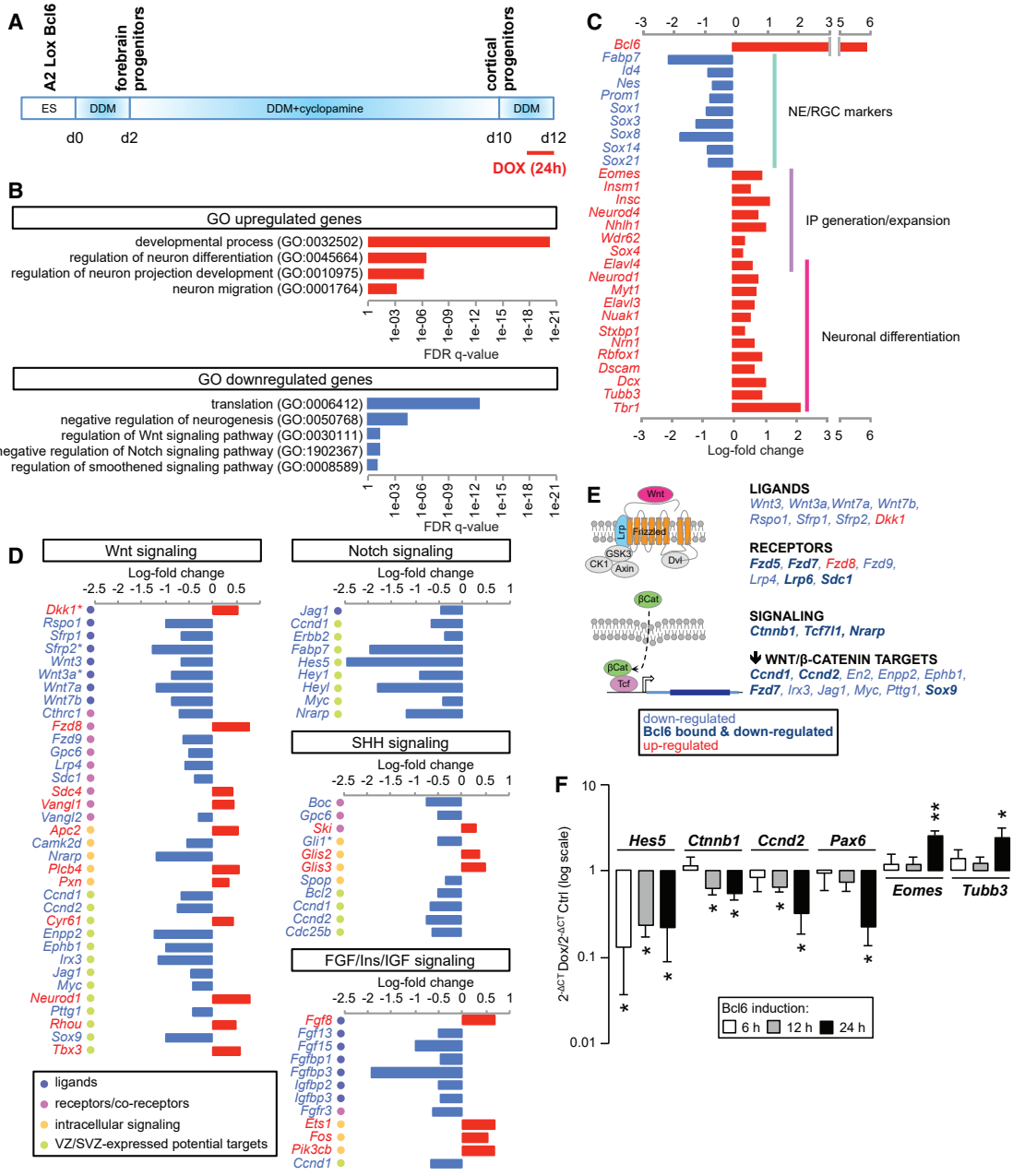

Figure 1. Bcl6 Promotes a Neurogenic Transcription Program and Represses Selective Genes of the Main Proliferative Pathways

(A) Scheme representing the differentiation protocol of Bcl6-inducible A2 lox.Cre mouse embryonic stem cells into cortical progenitors. Bcl6 expression was induced at day 12 using a single doxycycline pulse for 24 h.

(B) Gene Ontology analysis showing statistically significant enrichment for some categories of up- and downregulated genes following Bcl6 induction (see also Table S2 for complete lists).

(C) Histograms representing the log-fold change of a series of significantly up- or downregulated genes, respectively indicated in red or blue, selected upon their expression and/or function during cortical differentiation. IP, intermediate progenitors; NE, neuroepithelial cells; RGC, radial glial cells (see also Table S1 for complete lists).

(D) Histograms representing the log-fold change of significantly up- or downregulated genes, respectively indicated in red or blue, belonging to the main proliferative pathways in cortical progenitors. Only the potential target genes with known expression in embryonic cortical progenitors are indicated. For the complete list of genes taken into consideration for the analysis, see also Table S3. Genes marked with an asterisk also are target genes of the pathway itself. SVZ, subventricular zone; VZ, ventricular zone.

(E) Scheme of the canonical Wnt pathway depicting the role in the cascade of the ensemble of Wnt/β-catenin-related genes bound and/or altered by Bcl6 investigated in this study.

(legend continued on next page)

activity (Kim et al., 2009). Also, some key effectors genes, such as *Cyclin d1/d2*, are found as common targets of all morphogen pathways, depending on cellular context (Cohen et al., 2010; Kalita et al., 2013; Katoh and Katoh, 2009; Nilsson et al., 2012; Shtutman et al., 1999). How these intermingled pathways are effectively shut down during neurogenesis is therefore a complex issue and remains largely unresolved.

We previously reported that the transcriptional repressor Bcl6 (Baron et al., 1993; Chang et al., 1996) is required for neuronal differentiation in the cerebral cortex and directly represses the Notch-dependent *Hes5* target (Tiberi et al., 2012a), and in the cerebellum, Bcl6 promotes neurogenesis through repression of SHH pathway effectors *Gli1/2* (Tiberi et al., 2014). This raises the question whether Bcl6 promotes neurogenic conversion through the repression of distinct targets, depending on the cellular context, or through a more generic transcriptional repression program.

Here, we combine transcriptome, epigenome, and *in vivo* functional analyses to determine the molecular logic of action of Bcl6 during neurogenesis, focusing on the cerebral cortex. We find that Bcl6 acts as a global repressor of a repertoire of signaling components of most signaling pathways known to promote self-renewal, including Notch, SHH, FGF, and most strikingly the Wnt pathway. These data define a molecular logic of neurogenesis whereby a single intrinsic factor downregulates the responsiveness to extrinsic cues, through transcriptional repression at multiple parallel and serial levels along these pathways, to ensure irreversible neurogenic fate transition.

RESULTS

Bcl6 Upregulates an Intrinsic Neurogenic Program and Downregulates Extrinsic Proliferative Pathways

To determine the primary molecular mechanisms of Bcl6 action in cortical neurogenesis, we performed RNA sequencing (RNA-seq) transcriptome analysis on *in vitro* embryonic-stem-cell-derived cortical progenitors driving inducible Bcl6 expression in order to timely control the transgene induction (Figure 1A; Gaspard et al., 2008; Tiberi et al., 2012a). We found that, 24 h following Bcl6 induction, 764 genes were significantly upregulated, with *Bcl6* being the most increased, and 610 genes were significantly downregulated, with *Hes5* being the most repressed (Table S1).

Gene Ontology analysis of the upregulated genes revealed a significant enrichment in categories linked to development and cell or neuron differentiation (Figure 1B; Table S2). More specifically, most of the canonical markers of differentiation into intermediate progenitors and neurons were significantly upregulated (Figure 1C; Table S1). On the other hand, downregulated genes showed an enrichment in gene categories linked to regulation of translation, negative regulation of neurogenesis, and most strikingly to signaling pathways promoting the expansion and self-renewal of cortical progenitors (Figure 1B; Table S2). Among the significantly downregulated genes, we found, as expected, markers of radial glial cells and transcriptional targets of Notch but also many signaling components of FGF and SHH-dependent pathways and, most strikingly, a high number of genes belonging to the Wnt signaling cascade, from ligands to receptors to target genes (Figures 1C–1E; Tables S1 and S3). Given that Bcl6 has strong effects on neurogenesis, it could be that these global transcriptional changes reflect the consequence of changes in cell fate rather than direct regulation by Bcl6. However, the majority of the tested genes belonging to these proliferative pathways (8/11) were downregulated following Bcl6 induction several hours earlier than changes in cell fate markers (Figures 1F and S1A), indicating that their downregulation is not the mere result of Bcl6-mediated differentiation.

Bcl6 Functionally Alters β-Catenin/Tcf Signaling to Promote Neurogenesis

Given the importance of the Wnt pathway in the regulation of self-renewal versus differentiation balance in the cortex (Chenn and Walsh, 2002; Fang et al., 2013; Hirabayashi and Gotoh, 2005; Hirabayashi et al., 2004; Kuwahara et al., 2010; Munji et al., 2011; Mutch et al., 2010; Wrobel et al., 2007; Zhang et al., 2010) and the number of downregulated genes belonging to this pathway, we tested the global impact of Bcl6 on the Wnt pathway *in vivo*. *Axin 2*, a classical Wnt/β-catenin-dependent target gene, was found to be upregulated in *Bcl6*$^{-/-}$ mouse embryonic cortex using *in situ* hybridization. Although *Axin2* expression is normally detected in the medial pallium of the frontal cortex in wild-type animals, a higher signal was found throughout dorsolateral levels in *Bcl6*$^{-/-}$ mice (Figures 2A and 2B), suggesting that β-catenin/Tcf activity is increased in the mutant cortex. Interestingly, this difference was not detectable at more posterior levels (Figures 2A and 2B), in accordance with the frontal high occipital low graded *Bcl6* expression (Tiberi et al., 2012a). Given that these gene expression changes are specific to the frontal cortex, we tested whether they could affect areal patterning in the mutant mice. However, analysis of the pattern of expression of several area-specific markers did not detect any obvious changes in areal patterning in the *Bcl6* mutant mice (Figures S2A–S2J), suggesting that Bcl6 effect on the Wnt pathways does not affect regional patterning of the cortex.

On the other hand, these data suggest that Bcl6 neurogenic function could depend on the downregulation of the canonical Wnt pathway. We first tested this *in vitro* by examining potential genetic interactions between Bcl6 and β-catenin, the main signaling hub protein of the pathway. Neurogenic genes upregulated *in vitro* by Bcl6 were prevented by CHIR99021, a GSK3 inhibitor over-activating the canonical Wnt pathway. CHIR99021, which increased the levels of the Wnt reporter gene *Lef1*, also prevented Bcl6-mediated downregulation of Wnt target genes but did not prevent repression of Notch targets (Figure S2K).

(F) qRT-PCR analysis of the Notch target *Hes5*, Wnt-related genes *Ctnnb1* and *Ccnd2*, and the cell fate markers *Pax6*, *Eomes*, and *Tubb3* in day 12 *in vitro* cortical progenitor cells treated with DMSO (control) or doxycycline for 6, 12, or 24 h. Data are presented as mean + SEM of Dox over control (Ctrl) absolute levels (n = 7–9 [6 h], 27–30 [12 h], and 9 [24 h] from at least 3 independent differentiations for each group). *p < 0.05; **p < 0.01 using Student's t test. See also Figure S1.

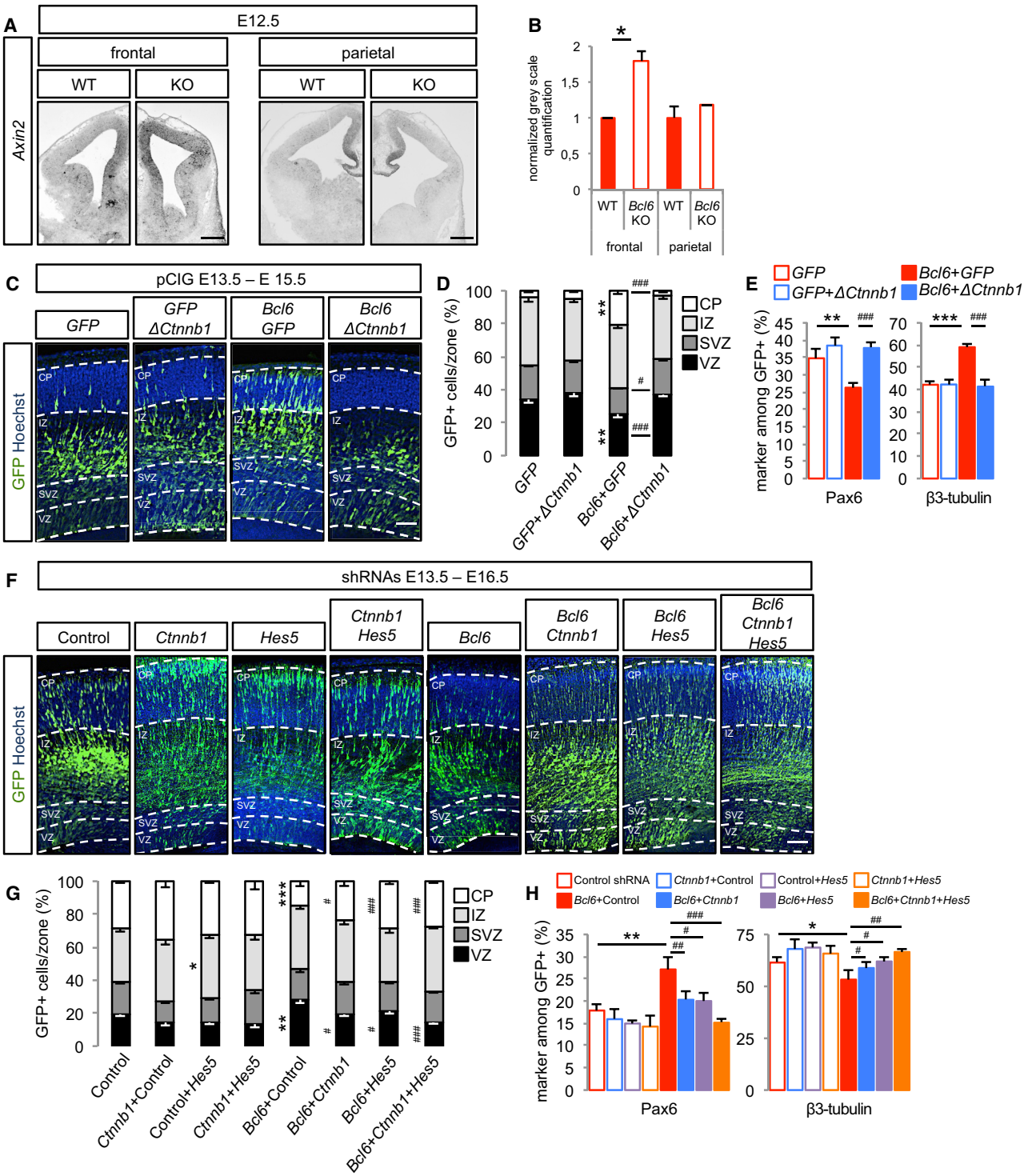

Figure 2. *Bcl6* Alters β-Catenin Signaling *In Vivo* to Promote Neurogenesis

(A) *In situ* hybridization of *Axin2* Wnt reporter gene on coronal sections of E12.5 wild-type and *Bcl6*$^{-/-}$ frontal and parietal telencephalon. Scale bars, 500 μm.

(B) Normalized gray scale quantifications of *Axin2* levels were performed using ImageJ software. Data are presented as mean + SEM. *p < 0.05 using Student's t test.

(C–E) *In utero* electroporation of pCIG, pCIG+pCAG-Δ(1-90)*Ctnnb1*, pCIG-*Bcl6*+pCIG or pCIG-*Bcl6*+pCAG-Δ(1-90)*Ctnnb1* at E13.5.

(C) Hoechst and GFP immunofluorescence was performed on coronal sections of E15.5 brains. Dashed lines mark the basal and apical margins of the VZ, SVZ, intermediate zone (IZ), and cortical plate (CP). Scale bar, 50 μm.

(legend continued on next page)

We then examined *in vivo* the impact of the gain of function of a stabilized β-catenin mutant on *Bcl6* overexpression using *in utero* electroporation. *Bcl6* gain of function alone led to increased neurogenesis, as assessed by increased number of cells in the cortical plate (CP) and an increase in Neurod2+ and Tuj1+ neurons, at the expense of ventricular zone (VZ)-located Pax6+ and Sox2+ progenitors, without detectable effect on neuronal migration or progenitor delamination (Figures 2C–2E and S3A–S3G). Importantly, these effects were suppressed by overexpression of stabilized β-catenin (Figures 2C–2E and S4C).

Conversely, we combined *Bcl6* and β-catenin (*Ctnnb1*) knockdown to assess potential epistasis. As expected (Tiberi et al., 2012a), *Bcl6* knockdown led to decreased neurogenesis per se, as reflected by increased cell number in the VZ at the expense of the CP, associated with increased levels of radial glial cell progenitors and decreased neurons (Figures 2F–2H and S3H–S3N), and this phenotype was significantly rescued by the *Ctnnb1* knockdown (Figures 2F–2H).

These data collectively suggest that Bcl6 functionally acts on the Wnt pathway to promote neurogenesis, in addition to its effect on the Notch target *Hes5* (Tiberi et al., 2012a). We next directly compared the impact of Bcl6 on Wnt and Notch pathways *in vivo* by combining *Ctnnb1* and *Hes5* short hairpin RNAs (shRNAs) to further assess whether Bcl6 represses them in parallel or sequentially. *Hes5* knockdown rescued some of the *Bcl6* loss-of-function-mediated phenotype to levels similar to the rescue obtained using the *Ctnnb1* knockdown. However, the association of both *Ctnnb1* and *Hes5* shRNAs showed additive rescue of *Bcl6* knockdown, reaching the corresponding control levels (*Ctnnb1*+*Hes5* shRNA combination; Figures 2F–2H), suggesting that Bcl6 alters these two cascades at least in part in parallel.

Altogether, these data indicate that Bcl6-mediated repression of the Wnt pathway, already at the level of β-catenin, is necessary to elicit neurogenic activity, in parallel to Notch signaling repression. Thus, Bcl6 acts by repression of multiple pathways promoting progenitor self-renewal and proliferation.

As β-catenin is not only a key component of the Wnt pathway but also an important regulator of adherens junctions (Nelson and Nusse, 2004), we tested further the specific implication of the Wnt pathway by focusing on *Tcf7l1*, which was also found to be downregulated in response to Bcl6 *in vitro* (Figure S1A) and is the most heavily expressed Tcf/Lef transcription factor in cortical progenitors (Galceran et al., 2000).

Remarkably, we found that overexpression of *Tcf7l1* blocked Bcl6-mediated neurogenesis *in vivo* (Figures S4A–S4D). Hence, these data strongly suggest that β-catenin downregulation by Bcl6 is mostly linked to its Wnt-related transcriptional activity rather than its activity in adherens junctions. This is in line with our RNA-seq analyses, which show that the expression of most genes related to adherens junctions tend to increase upon Bcl6 overexpression, especially *Jup*/γ-catenin (Figure S1B), thereby compensating β-catenin decrease, as previously reported (Wickline et al., 2013).

Bcl6 Promotes Neurogenesis through Cyclin D Inhibition

Although Bcl6 appears to repress multiple serial components of individual pathways, it could also act through common effectors of parallel signals. In line with this hypothesis, *Cyclin d1/d2* genes were found to be downregulated by Bcl6 overexpression *in vitro* (Figure 1D; Table S1) and are known to be upregulated by pathways driving progenitor self-renewal, including Wnt (Shtutman et al., 1999) but also SHH (Kasper et al., 2006; Katoh and Katoh, 2009), FGF-insulin growth factor (IGF) (Kalita et al., 2013; Nilsson et al., 2012), and Notch (Cohen et al., 2010). Moreover, Cyclin d1/d2 are key promoters of cortical progenitor proliferation and consequently block neurogenesis (Lange et al., 2009; Pilaz et al., 2009; Tsunekawa et al., 2012).

We first examined their expression in the developing cortex in wild-type and *Bcl6*$^{-/-}$ brains. *Ccnd1* was found in the VZ and SVZ in wild-type mice as previously reported (Glickstein et al., 2007), and its levels were significantly increased in *Bcl6*$^{-/-}$ animals (Figures 3A and 3B). *Ccnd2* mRNA was mostly detected in basal endfeet of radial glial cells and at lower intensity in the ventricular zone at embryonic day 12.5 (E12.5), as previously described (Tsunekawa et al., 2012). Although the high density of labeling and limited resolution of *in situ* hybridization precluded detecting upregulation in the basal endfeet, *Ccnd2* levels were significantly increased in the VZ in *Bcl6*$^{-/-}$ cortex (Figures 3C and 3D). Hence, *Bcl6* negatively controls *Ccnd1/2* expression in cortical progenitors *in vivo*. We next examined the functional impact of *Bcl6* loss of function on *Ccnd1*/*Ccnd2* double knockdown, as these two cyclins regulate cell cycle

(D) Histograms show the percentage of GFP+ cells in VZ, SVZ, IZ, and CP. $^{**}p < 0.01$ pCIG-*Bcl6*+pCIG versus pCIG and $^{\#}p < 0.05$, $^{\#\#\#}p < 0.001$ pCIG-*Bcl6*+pCAG-Δ(1-90)*Ctnnb1* versus pCIG-*Bcl6*+pCIG using two-way ANOVA followed by Tukey post hoc test.

(E) Histograms show the percentage of Pax6+ and Tuj1+ cells among the GFP+ cells. $^{**}p < 0.01$, $^{***}p < 0.001$ pCIG-*Bcl6*+pCIG versus pCIG+pCIG and $^{\#\#\#}p < 0.001$ pCIG-*Bcl6*+pCAG-Δ(1-90)*Ctnnb1* versus pCIG-*Bcl6*+pCIG using one-way ANOVA followed by Tukey post hoc test.

Data are presented as mean + SEM of n = 6 control embryos (1,856 cells), n = 10 embryos for stabilized β-catenin gain of function (2,727 cells), n = 9 embryos for Bcl6 gain of function (1,922 cells), and n = 9 embryos for Bcl6 and stabilized β-catenin double gain of function (1,588 cells).

(F–H) *In utero* electroporation of scramble (control), scramble+*Ctnnb1*, scramble+*Hes5*, scramble+*Ctnnb1*+*Hes5*, scramble+*Bcl6*, scramble+*Ctnnb1*+*Bcl6*, scramble+*Hes5*+*Bcl6*, and *Ctnnb1*+*Hes5*+*Bcl6* shRNAs at E13.5.

(F) Representative images of Hoechst and GFP immunofluorescence performed on coronal sections of E16.5 brains. Dashed lines mark the basal and apical margins of the VZ, SVZ, IZ, and CP. Scale bar, 50 μm.

(G) Histograms show the percentage of GFP+ cells in VZ, SVZ, IZ, and CP. $^{*}p < 0.05$, $^{**}p < 0.01$, $^{***}p < 0.001$ versus control and $^{\#}p < 0.05$, $^{\#\#\#}p < 0.001$ versus *Bcl6*+control shRNAs using two-way ANOVA followed by Tukey post hoc test.

(H) Histograms show the percentage of Pax6+ and β3-tubulin+ cells among the GFP+ cells. $^{*}p < 0.05$, $^{**}p < 0.01$ versus control and $^{\#}p < 0.05$, $^{\#\#}p < 0.01$, $^{\#\#\#}p < 0.001$ versus *Bcl6*+control shRNAs using one-way ANOVA followed by Tukey post hoc test.

Data are presented as mean + SEM of n = 15 control embryos (4,476 cells), n = 7 embryos for *Ctnnb1* shRNA (1,851 cells), n = 13 embryos for *Hes5* shRNA (3,893 cells), n = 7 embryos for *Ctnnb1*+*Hes5* shRNA (1,932 cells), n = 6 embryos for *Bcl6* shRNA (2,093 cells), n = 9 embryos for *Bcl6*+*Ctnnb1* shRNA (2,642 cells), n = 10 embryos for *Bcl6*+*Hes5* shRNA (2,614 cells), and n = 9 embryos for *Bcl6*+*Ctnnb1*+*Hes5* shRNA (2,993 cells).

See also Figures S2, S3, and S4.

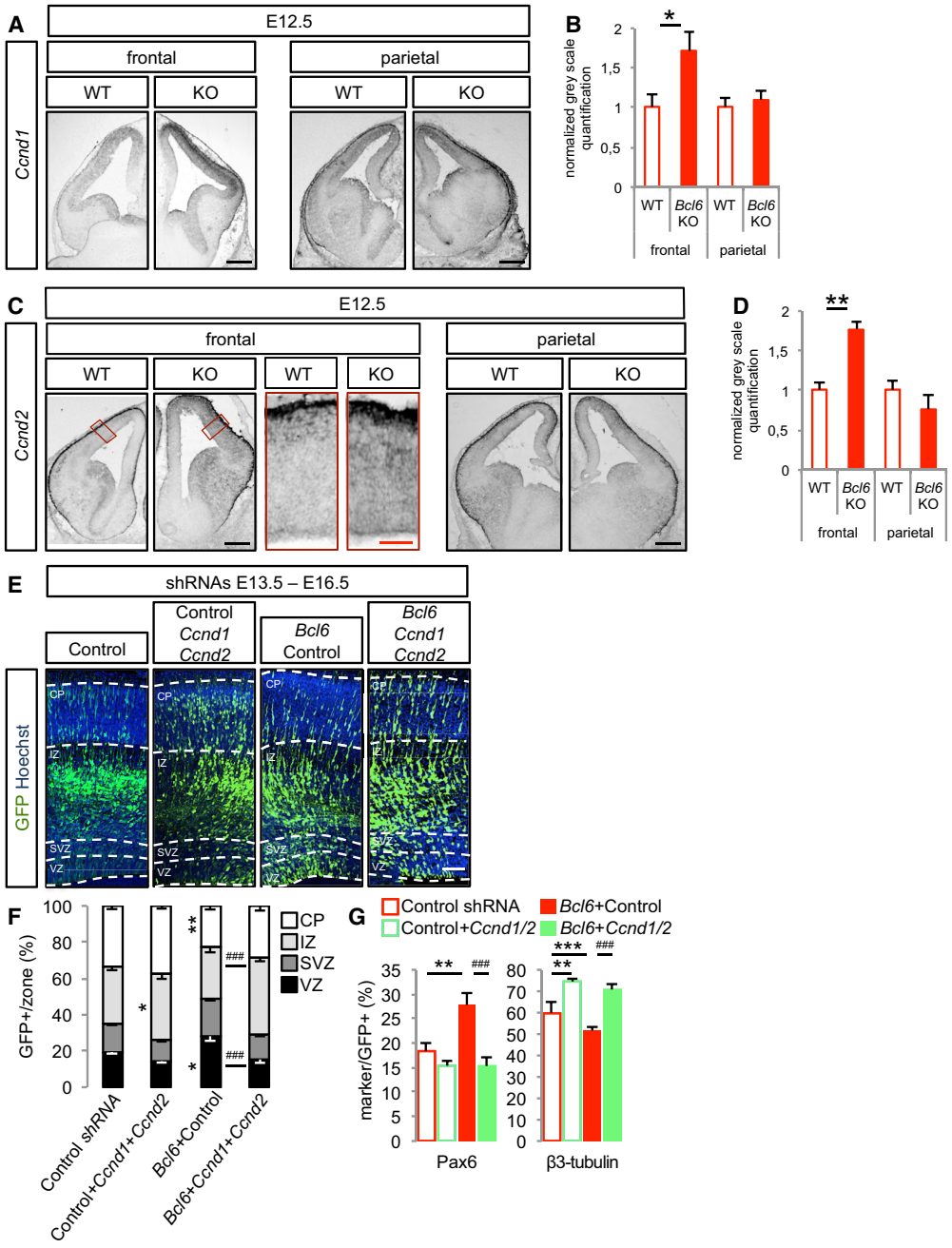

Figure 3. *Bcl6* Directly Affects *Ccnd1*/*Ccnd2* Expression *In Vivo* to Promote Neurogenesis

(A–D) *In situ* hybridization of (A) *Ccnd1* and (C) *Ccnd2* genes on coronal sections of E12.5 wild-type and *Bcl6*$^{-/-}$ frontal and parietal telencephalon. Normalized gray scale quantifications of (B) *Ccnd1* and (D) *Ccnd2* levels were performed using ImageJ software. Data are presented as mean + SEM. *$p < 0.05$, **$p < 0.01$ using Student's t test. Black scale bars, 500 μm. Red scale bar, 100 μm.

(E–G) *In utero* electroporation of scramble (control), scramble+*Ccnd1*+*Ccnd2*, scramble+*Bcl6*, and *Ccnd1*+*Ccnd2*+*Bcl6* shRNAs at E13.5.

(E) Representative images of Hoechst and GFP immunofluorescence performed on coronal sections of E16.5 brains. Dashed lines mark the basal and apical margins of the VZ, SVZ, IZ, and CP. Scale bar, 50 μm.

(F) Histograms show the percentage of GFP+ cells in VZ, SVZ, IZ, and CP. *$p < 0.01$, **$p < 0.01$ versus control and $^{###}p < 0.001$ versus *Bcl6*+control shRNAs using two-way ANOVA followed by Tukey post hoc test.

(G) Histograms show the percentage of Pax6+ and β3-tubulin+ cells among the GFP+ cells. **$p < 0.01$, ***$p < 0.001$ versus control and $^{###}p < 0.001$ versus *Bcl6*+control shRNAs using one-way ANOVA followed by Tukey post hoc test.

Data are presented as mean + SEM of n = 12 control embryos (3,627 cells), n = 7 embryos for *Ccnd1*+*Ccnd2* shRNA (1,519 cells), n = 8 embryos for *Bcl6* shRNA (1,998 cells), and n = 12 embryos for *Bcl6*+*Ccnd1*+*Ccnd2* shRNA (3,475 cells).

See also Figures S3 and S4.

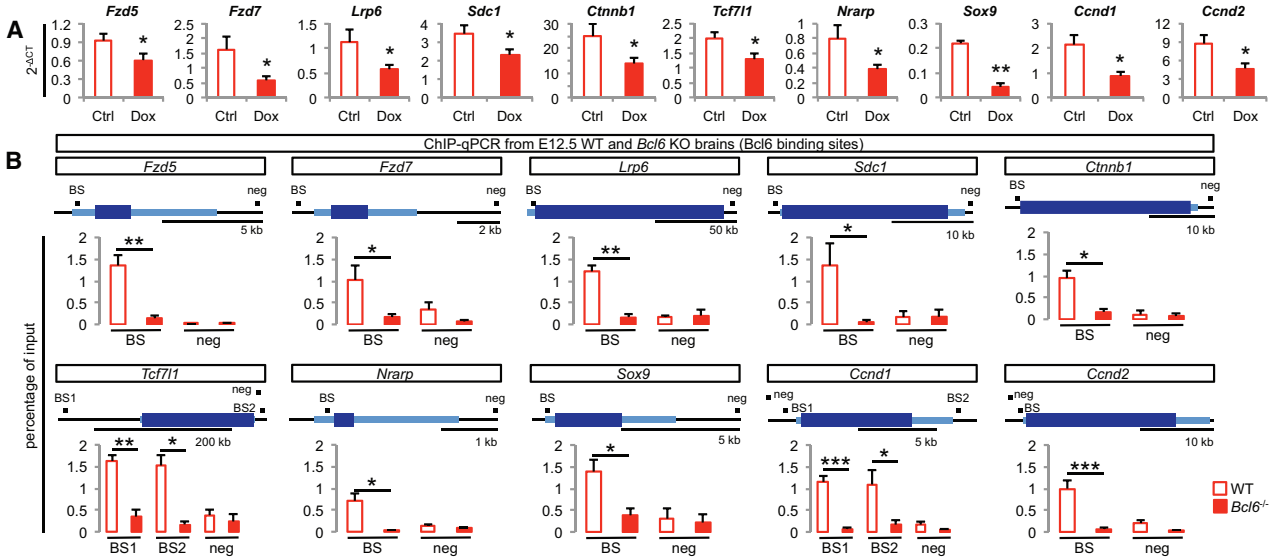

Figure 4. Bcl6 Binds to Core Genes of the Wnt/β-Catenin Pathway to Alter Their Expression

(A) qRT-PCR analysis of Wnt-related genes from DMSO- and doxycycline-treated cells at day 12. Data are presented as mean + SEM of absolute levels (n = 21 from 8 differentiations). *p < 0.05 and **p < 0.01 using Student's t test.

(B) ChIP-qPCR validation of screened Bcl6-binding sites on regulatory regions and negative control sites of significantly downregulated Wnt-related genes in E12.5 wild-type and *Bcl6*$^{-/-}$ telencephalon using a Bcl6 antibody. Data are presented as mean + SEM of input enrichment (n = 4). *p < 0.05, **p < 0.01, and ***p < 0.001 using Student's t test. Genes are represented using 5′ to 3′ orientation with light blue showing 5′ UTR and 3′ UTR exons and thicker dark blue showing the exons of the coding sequence and the introns according to RefSeq gene sequences from mouse genome mm10 assembly (https://genome.ucsc.edu). Black boxes indicate amplified regions (BS, region comprising the Bcl6-predicted binding site inside the ChIP-seq significant peaks; NEG, region with no predicted Bcl6 matrix using the Jaspar software [http://jaspar.genereg.net]).

See also Figures S5 and S6.

progression in a redundant manner (Ciemerych et al., 2002; Glickstein et al., 2007; Tsunekawa et al., 2012). Decreased neurogenesis observed following *Bcl6* shRNA was completely rescued by the dual *Ccnd1*/*Ccnd2* knockdown (Figures 3E–3G and S4E–S4G). Conversely, *Ccnd1* overexpression blocked Bcl6-elicited neurogenesis *in vivo* (Figures S4A–S4D). This indicates that, in addition to repressing specific signaling pathway components, Bcl6 action also involves repression of common terminal effector targets, such as *Ccnd1/2*, driving progenitor proliferation and self-renewal.

Bcl6 Represses Transcription through Sirt1-Mediated Histone Deacetylation as well as Target-Specific Mechanisms

Overall, our data indicate that Bcl6 acts through inhibition of multiple pathways to promote neurogenesis, raising the question of which effects are directly related to Bcl6 transcriptional repression or reflect its indirect consequences. To address this point, we performed chromatin immunoprecipitation (ChIP)-seq to identify Bcl6 binding sites using *in vitro* cortical progenitors driving inducible Bcl6 expression in order to increase the efficiency of the immunoprecipitation (Figure S5). This revealed that Bcl6 binding was predominantly found on promoter regions, with a significant enrichment for Bcl6 matrix binding motif (Figures S5A–S5D). Further, 39% of the Bcl6-predicted targets (1,701/4,366 peak-associated genes) were similar to those previously reported by ChIP-seq in human B cells (Basso et al., 2010). In line with our transcriptomics data, Bcl6 bound to numerous genes of the multiple cascades regulating the proliferation of cortical progenitors (Figure S5E), although it should be noted that only 19% of the downregulated genes from the RNA-seq dataset were found in the ChIP-seq screen (115/610 genes), indicating partial discrepancy between transcription factor binding and transcriptional effect, at least at the time points tested.

Then we validated *in vivo* some of these targets using ChIP-qPCR on the identified binding peaks in E12.5 wild-type and *Bcl6*$^{-/-}$ cortex, focusing on Wnt and Notch pathways. We first confirmed Bcl6 binding to the Notch target *Hes5* but also identified additional Bcl6/Notch targets, such as *Hes1* and *Nrarp* (Figures 4 and S6A). Moreover, we found that Bcl6 bound to a repertoire of VZ-expressed genes of the Wnt/β-catenin cascade as well as potential Wnt/β-catenin targets, among which 10 showed significant downregulation upon Bcl6 induction in *in vitro* embryonic stem cell (ESC)-derived cortical progenitors, whether by RNA-seq or qRT-PCR, suggesting a direct functional impact following Bcl6 binding (Figures 4A and S6D). The genes bound and regulated by Bcl6 ranged from Wnt receptors and co-receptors to intracellular effectors to Wnt target genes (Figures 1E, 4B, and S6E).

We next examined how Bcl6 binding to its target sequences might lead to transcriptional repression. We previously found that Bcl6-mediated *Hes5* repression occurs through modifications of histone acetylation mediated by Sirt1 deacetylase recruitment (Tiberi et al., 2012a). Remarkably, we found a similar

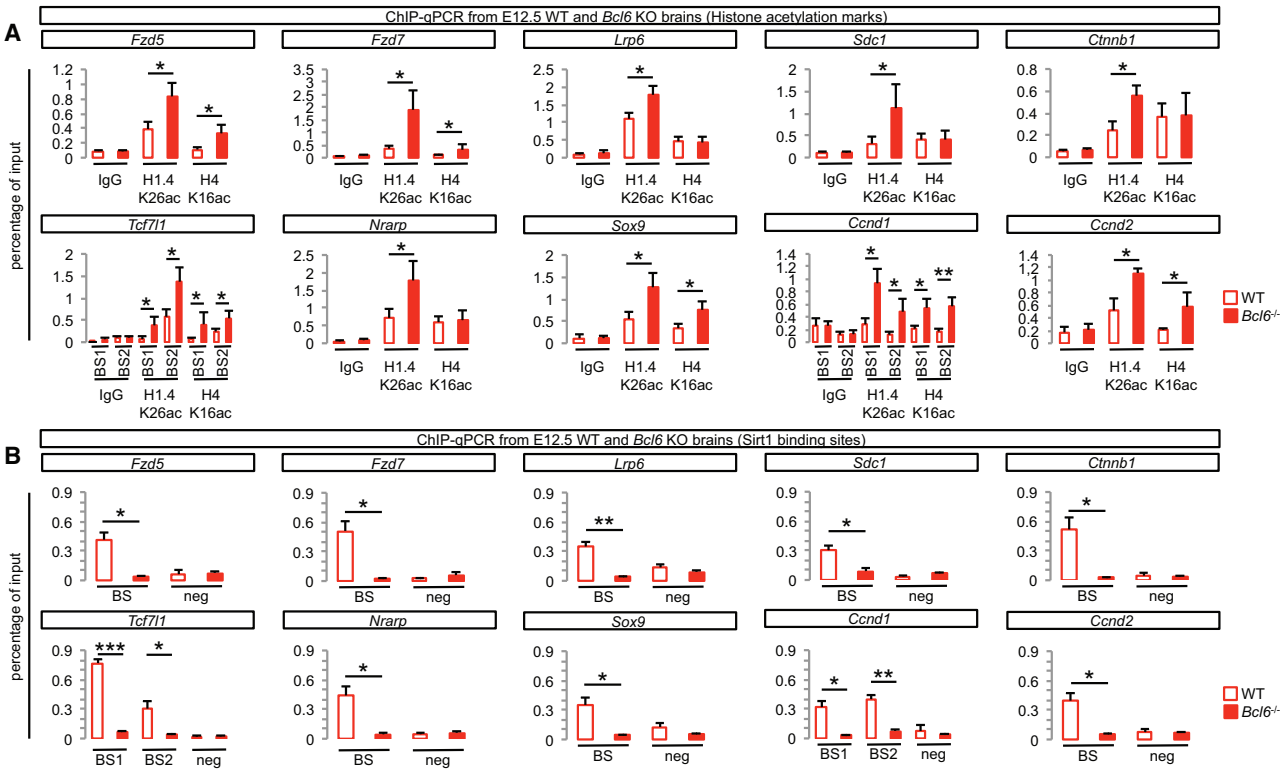

Figure 5. Bcl6 Binding to Significantly Downregulated Wnt-Related Genes Induces Chromatin Remodeling and Sirt1 Recruitment

(A) ChIP-qPCR of histone acetylation marks on Bcl6 binding sites of significantly downregulated Wnt-related genes in E12.5 wild-type and *Bcl6*$^{-/-}$ telencephalon using control (rabbit immunoglobulin G [IgG]) and H1.4K26ac and H4K16ac antibodies. Data are presented as mean + SEM of input enrichment (n = 6). *p < 0.05 and **p < 0.01 using Student's t test.

(B) ChIP-qPCR on validated Bcl6 binding sites of significantly downregulated Wnt-related genes in E12.5 wild-type and *Bcl6*$^{-/-}$ telencephalon using a Sirt1 antibody. Data are presented as mean + SEM of input enrichment (n = 6). *p < 0.05, **p < 0.01, and ***p < 0.001 using Student's t test.

See also Figure S6.

mechanism for all tested target genes identified above (Figure 5). Indeed, *in vivo* ChIP-qPCR experiments performed on mouse E12.5 embryonic cortex showed enrichment for acetylated lysines H4K16 and H1.4K26 on all tested genes in *Bcl6*$^{-/-}$ cortex compared with wild-type, indicating that repressive chromatin remodeling required the presence of Bcl6 binding (Figures 5A and S6B). Moreover, we detected binding of the histone deacetylase Sirt1 to all Bcl6-bound target genes, which was abolished in *Bcl6*$^{-/-}$ cortex (Figures 5B and S6C).

To test whether Sirt1 activity was indeed required for Bcl6 activity, we examined in more depth the transcriptional regulation of *Ccnd1/2.* Bcl6 was found to bind to their regulatory regions *in vitro*, together with Sirt1, in association with histone H4K16 deacetylation, as observed *in vivo* (Figure 6). Furthermore, we found that sirtuin activity inhibition effectively blocked the Bcl6-mediated *Ccnd1/2* downregulation, confirming the importance of Sirt1-dependent histone deacetylation in the repression of these genes by Bcl6 (Figure S7A).

These data point to a generic mechanism by which a wide repertoire of the genes downregulated by Bcl6 and belonging to stem-cell-renewal signaling pathways are directly bound and repressed by Bcl6, which then recruits Sirt1, leading to their transcriptional silencing.

On the other hand, given the important role of Tcf7l1 in Bcl6 effects on neurogenesis, we examined in more detail the chromatin binding profiles of Tcf7l1 on the *Ccnd1/2* regulatory regions (Figure 6). This revealed that Tcf7l1 bound to both *Ccnd1/2* promoters on predicted Tcf/Lef binding sites, confirming their direct link with the Wnt pathway (Figure 6). Remarkably, this binding was decreased upon Bcl6 overexpression (Figure 6B). In contrast, Tcf7l1 binding at the level of the *Lef1* promoter, to which Bcl6 does not bind to, was unaffected (Figures S7B and S7C). These data thus suggest that Bcl6 directly affects Tcf7l1 binding in a target-specific way, as an additional selective mechanism to modulate Wnt-dependent gene expression.

DISCUSSION

Neurogenesis is a key fate transition controlled by the interplay of intrinsic and extrinsic cues, but how these are integrated at the molecular level remains mostly unknown. Here, we identify the Bcl6 transcriptional repressor as a neurogenic factor that acts through the direct repression of a repertoire of genes encoding key components of numerous extrinsic morphogen pathways that promote self-renewal and proliferation of cortical progenitors,

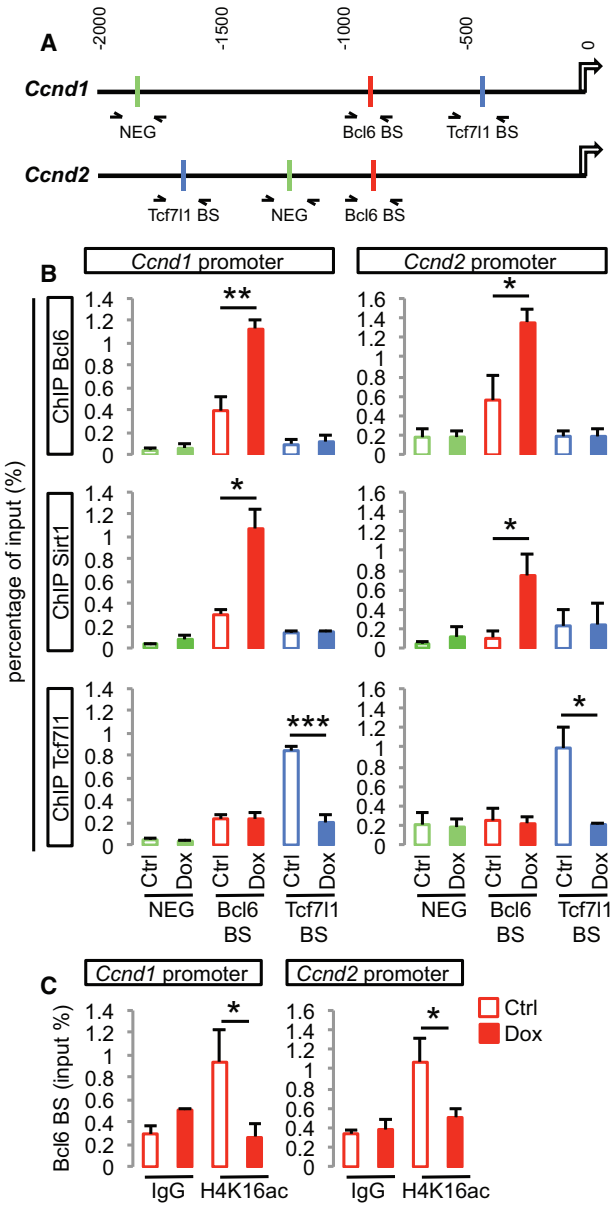

Figure 6. Bcl6 and Sirt1 Bind to *Ccnd1* and *Ccnd2* Regulatory Regions, Leading to the Removal of the β-Catenin Effector Tcf7l1

(A) Schematic representation of the genomic region 2 kb upstream of *Ccnd1* and *Ccnd2* transcription starting sites showing validated Bcl6 (red) as well as putative Tcf7l1 (blue) binding sites and negative regions for either transcription factor (green) as predicted by the Jaspar software (http://jaspar.genereg.net). The arrows represent the amplified regions by qPCR used to measure the enrichment following ChIP.

(B) ChIP-qPCR analysis of the Bcl6, Sirt1, and Tcf7l1 binding sites on the *Ccnd1* and *Ccnd2* regulatory regions in cortical progenitors derived from *Bcl6* A2 lox.Cre mouse ESCs (differentiation day 12, 24 h DMSO [Ctrl] or Dox treatment). Data are presented as mean + SEM of input enrichment (n = 3 differentiations). *p < 0.05, **p < 0.01, and ***p < 0.001 using Student's t test.

(C) ChIP-qPCR analysis of the H4K16ac histone acetylation mark on Bcl6 binding sites of the *Ccnd1* and *Ccnd2* regulatory regions in cortical progenitors derived from *Bcl6* A2 lox.Cre mouse ESCs (differentiation day 12, 24 h DMSO [Ctrl] or Dox treatment). Data are presented as mean + SEM of input enrichment (n = 3 differentiations). *p < 0.05 using Student's t test.

See also Figure S7.

most strikingly the Wnt pathway. This provides important insight on the molecular logic by which neurogenic conversion can occur in a robust fashion in the presence of many, and sometimes contradictory, extrinsic cues.

Our transcriptome analysis shows that Bcl6 gain of function elicited a broad neurogenic program, from genes involved in the generation and expansion of intermediate progenitors to their differentiation into neurons, as well as neuronal maturation and specification, similarly to the response to the proneural *Neurog2* transcription factor in the developing cortex (Gohlke et al., 2008; Johnson et al., 2015). However, in the case of Bcl6, these effects are caused by a direct negative impact of Bcl6 on pathways promoting self-renewal and proliferation. Indeed, Bcl6 represses the transcription of genes related to most signaling cascades that favor the proliferation of cortical progenitors at the expense of their differentiation, most strikingly, the Notch and Wnt pathways, as well as SHH and FGF. Combining our RNA-seq results with ChIP experiments, we found that Bcl6 directly binds to most of these genes, leading to their transcriptional repression, even if future work will be needed to describe in depth Bcl6 direct repression on pathways other than Notch and Wnt.

This global effect is conceptually similar to the one previously proposed for Myt1l in the frame of neuronal reprogramming, where a single transcription factor appears to repress globally multiple non-neuronal fates to promote *in vitro* conversion into neurons (Mall et al., 2017). It is also complementary to the classical effects of the Rest complex, which represses neuronal fate genes in non-neuronal cells (Ballas et al., 2005). In the case of Bcl6, however, the repression does not appear to act on fate-specific genes per se but rather on specific genes involved in extrinsic signaling pathways promoting progenitor maintenance. In this sense, Bcl6 acts probably mostly during fate transition itself, and this molecular logic could thereby explain how neuronal differentiation takes place irreversibly, even in the presence of proliferative extrinsic cues, thus providing robustness to the neurogenesis processes.

Interestingly, in the case of Wnt signaling, Bcl6 appears to act upon multiple components, from receptors to transducers and transcriptional effectors, as attested by the functional interactions between Bcl6 and β-catenin and Tcf7l1, as well as with Ccnd1/2, revealed in this study. This implies that, although Bcl6 can alter the intracellular response of Notch signaling in a target-specific way (Sakano et al., 2010; Tiberi et al., 2012a), its effect on Wnt signaling appears to be much more global, from responsiveness to output. This may be related to the high complexity of the Wnt pathway, such as multiplicity of ligands and receptors and cell-dependent positive and negative feedback loops (Clevers and Nusse, 2012; MacDonald et al., 2009), on which acting at multiple levels of repression may be required to achieve its robust silencing. Indeed, it should be noted that, although many of the Wnt components that are repressed are positive regulators of the pathway, some inhibitors of the

pathway, such as *Sfrp1/2*, were also downregulated, and some activators, such as *Fzd8*, or inhibitors, such as *Dkk1*, were, most likely indirectly, upregulated. The same is true for the other examined morphogen pathways, thus suggesting that, although the overall effect of Bcl6 on these pathways is inhibitory, the net effect on some individual genes could sometimes result in transcriptional activation.

Moreover, the comparison of combined epistasis of *Bcl6* with *Hes5* and *Ctnnb1* revealed that Bcl6 appears to affect Notch and Wnt signaling in a parallel fashion rather than through a cascade of events following the alteration of a single upstream pathway. Furthermore, some Bcl6-elicited gene expression changes impact several pathways at the same time. For instance, we observed that Bcl6 gain of function decreases the expression of *Jag1* and *Nrarp*, which are both linked to Notch but also Wnt pathways (Ishitani et al., 2005; Phng et al., 2009).

We identify *Ccnd1* and *Ccnd2* as major key targets of Bcl6, and their downregulation rescues to a large extent the loss of *Bcl6*. *Ccnd1* or *Ccnd2* were previously shown to act as key promoters of cortical progenitor proliferation and blockers of differentiation (Lange et al., 2009; Pilaz et al., 2009; Tsunekawa et al., 2012) and are found downstream of most signaling pathways promoting progenitor self-renewal. This suggests a model whereby Bcl6 contributes to robustness of fate transition by also acting on key common downstream targets.

In principle, *Ccnd1/2* regulation by Bcl6 could contribute to other aspects of cortical development, such as area patterning (Miyama et al., 1997), given Bcl6 preferential expression in the frontal cortex and its effects on signaling cues, such as Wnts and FGFs that can also impact on cortical areal patterning (Sur and Rubenstein, 2005; Tiberi et al., 2012a). However, our analyses of the cortex of *Bcl6* knockout mice failed to reveal any alteration in areal patterning, indicating that Bcl6 essential function is on the regulation of neurogenesis itself.

From a molecular viewpoint, Bcl6 appears to act through the same generic mechanism on most, if not all, of its targets, i.e., direct repression and Sirt1 recruitment, together with histone deacetylation that is correlated with decreased transcription. Interestingly, Bcl6 expression is progressively increased during the transition of radial glia cells into neurons either directly or indirectly though the generation of intermediate progenitors (Tiberi et al., 2012a), and Sirt1 expression appears to be constant in all cell types during cortical development (Ayoub et al., 2011; Loo et al., 2019). Thus, the induction of Bcl6 expression and/or post-transcriptional mechanisms could precisely regulate the activity of the Bcl6-Sirt1 complex during the neurogenic transition; it will be interesting to identify whether this relies on extrinsic cues or intrinsic factors.

One striking effect of Bcl6 is direct repression of β-catenin, which is a key mediator of the Wnt pathway but also a critical regulator of adherens junctions, which are essential for proper function of radial glia progenitors (Götz and Huttner, 2005). It is therefore critical to disentangle the involvement of β-catenin either on cell adhesion or Wnt signaling (Valenta et al., 2011). In this frame, our data point to the conclusion that Bcl6-mediated repression of β-catenin to induce neurogenesis is mostly related to Wnt-dependent transcription and not on adherens junction regulation, which are likely to be maintained despite β-catenin downregulation through compensatory mechanisms, such as upregulation of γ-catenin (Wickline et al., 2013).

Moreover, in relation with β-catenin transcriptional activity, our data indicate that Tcf7l1 is a key mediator of Wnt signaling that is directly downstream of Bcl6. Wnt activation has been reported to have differential effects on neurogenesis (Chenn and Walsh, 2002; Fang et al., 2013; Hirabayashi and Gotoh, 2005; Hirabayashi et al., 2004; Kuwahara et al., 2010; Munji et al., 2011; Mutch et al., 2010; Wrobel et al., 2007; Zhang et al., 2010), and Tcf7l1 was previously proposed to act either as a repressor or an activator of transcription of Wnt-specific genes (Cole et al., 2008; Kim et al., 2000; Lu et al., 2015; Shy et al., 2013; Wu et al., 2012; Yi et al., 2011). However, our data indicate that, in the context of Bcl6 effects on neurogenesis, Tcf7l1 acts mostly as a blocker of neurogenesis, in line with previous findings (Ohtsuka et al., 2011), and thereby likely as an activator of pro-proliferative genes, such as *Ccnd1/2* identified in this study.

To sum up, our data identify a major role for Bcl6 during neurogenesis by the direct transcriptional repression of most signaling pathways promoting cortical progenitor self-renewal. As Bcl6 is expressed in only specific subsets of progenitors and neurons during brain development, future work should determine whether and how other transcriptional repressors in other parts of the nervous system can modulate responsiveness to extrinsic cues to ensure robust and irreversible neurogenic fate transition.

STAR★METHODS

Detailed methods are provided in the online version of this paper and include the following:

- KEY RESOURCES TABLE
- LEAD CONTACT AND MATERIALS AVAILABILITY
- EXPERIMENTAL MODEL AND SUBJECT DETAILS
  - Animals
- METHOD DETAILS
  - In Utero Electroporation
  - Mouse ES cells and cortical differentiation
  - Plasmids
  - Immunofluorescence
  - Transcriptome analyses
  - RT-qPCR
  - *In situ* RNA hybridization
  - Chromatin Immunoprecipitation
  - ChIP-seq
- QUANTIFICATION AND STATISTICAL ANALYSIS
- DATA AND CODE AVAILABILITY

SUPPLEMENTAL INFORMATION

Supplemental Information can be found online at https://doi.org/10.1016/j.neuron.2019.06.027.

ACKNOWLEDGMENTS

The authors thank G. Vassart for continuous support and interest, members of the Vanderhaeghen lab and Institute for Interdisciplinary Research for helpful discussions and advice, J.-M. Vanderwinden of the Light Microscopy Facility for his support with imaging, F. Libert and A. Lefort (Brussels Interuniversity

Genomics High Throughput core) and D. Gacquer for RNA-seq, Dr. Raymond Poot for expert advice on ChIP-seq experiments, the Advanced Sequencing Team at the Francis Crick Institute for ChIP-seq, B. Merrill (University of Illinois) for kindly sharing Tcf7l1 antibody, and R. Dalla-Favera (Columbia University)for generously sharing the *Bcl6*$^{-/-}$ mice. This work was funded by the Belgian FRS/FNRS, the European Research Council (ERC Adv grant GENDEVOCORTEX), the FMRE, the Interuniversity Attraction Poles Program (IUAP), the WELBIO Program of the Walloon Region, the AXA Research Fund, the Fondation ULB, the ERA-net "Microkin" (to P.V.), and the Vlaams Instituut voor Biotechnologie (VIB) (to P.V. and S.A.). The work done in F.G.'s lab was funded by the Francis Crick Institute, which receives its core funding from Cancer Research UK (FC0010089), the UK Medical Research Council (FC0010089), and the Wellcome Trust (FC0010089).

AUTHOR CONTRIBUTIONS

Conceptualization and Methodology, J.B., L.T., J.v.d.A., and P.V.; Investigation, J.B. and L.T. with the help of J.v.d.A., Z.B.G., A.B., A.H., and F.D.V.B.; Formal Analysis, J.B., D.P., and X.L.; Writing – Original Draft, J.B. and P.V.; Writing – Review & Editing, J.B., L.T., J.v.d.A., D.P., F.G., S.A., and P.V.; Funding Acquisition, P.V.; Resources, F.G., S.A., and P.V.; Supervision, F.G., S.A., and P.V.

DECLARATION OF INTERESTS

The authors declare no competing interests.

Received: July 17, 2018
Revised: May 8, 2019
Accepted: June 26, 2019
Published: July 25, 2019

REFERENCES

Anders, S., Pyl, P.T., and Huber, W. (2015). HTSeq–a Python framework to work with high-throughput sequencing data. Bioinformatics *31*, 166–169.

Ayoub, A.E., Oh, S., Xie, Y., Leng, J., Cotney, J., Dominguez, M.H., Noonan, J.P., and Rakic, P. (2011). Transcriptional programs in transient embryonic zones of the cerebral cortex defined by high-resolution mRNA sequencing. Proc. Natl. Acad. Sci. USA *108*, 14950–14955.

Ballas, N., Grunseich, C., Lu, D.D., Speh, J.C., and Mandel, G. (2005). REST and its corepressors mediate plasticity of neuronal gene chromatin throughout neurogenesis. Cell *121*, 645–657.

Baron, B.W., Nucifora, G., McCabe, N., Espinosa, R., 3rd, Le Beau, M.M., and McKeithan, T.W. (1993). Identification of the gene associated with the recurring chromosomal translocations t(3;14)(q27;q32) and t(3;22)(q27;q11) in B-cell lymphomas. Proc. Natl. Acad. Sci. USA *90*, 5262–5266.

Basso, K., Saito, M., Sumazin, P., Margolin, A.A., Wang, K., Lim, W.K., Kitagawa, Y., Schneider, C., Alvarez, M.J., Califano, A., and Dalla-Favera, R. (2010). Integrated biochemical and computational approach identifies BCL6 direct target genes controlling multiple pathways in normal germinal center B cells. Blood *115*, 975–984.

Castro, D.S., Martynoga, B., Parras, C., Ramesh, V., Pacary, E., Johnston, C., Drechsel, D., Lebel-Potter, M., Garcia, L.G., Hunt, C., et al. (2011). A novel function of the proneural factor Ascl1 in progenitor proliferation identified by genome-wide characterization of its targets. Genes Dev. *25*, 930–945.

Chang, C.C., Ye, B.H., Chaganti, R.S., and Dalla-Favera, R. (1996). BCL-6, a POZ/zinc-finger protein, is a sequence-specific transcriptional repressor. Proc. Natl. Acad. Sci. USA *93*, 6947–6952.

Chenn, A., and Walsh, C.A. (2002). Regulation of cerebral cortical size by control of cell cycle exit in neural precursors. Science *297*, 365–369.

Ciemerych, M.A., Kenney, A.M., Sicinska, E., Kalaszczynska, I., Bronson, R.T., Rowitch, D.H., Gardner, H., and Sicinski, P. (2002). Development of mice expressing a single D-type cyclin. Genes Dev. *16*, 3277–3289.

Clevers, H., and Nusse, R. (2012). Wnt/β-catenin signaling and disease. Cell *149*, 1192–1205.

Cohen, B., Shimizu, M., Izrailit, J., Ng, N.F., Buchman, Y., Pan, J.G., Dering, J., and Reedijk, M. (2010). Cyclin D1 is a direct target of JAG1-mediated Notch signaling in breast cancer. Breast Cancer Res. Treat. *123*, 113–124.

Cole, M.F., Johnstone, S.E., Newman, J.J., Kagey, M.H., and Young, R.A. (2008). Tcf3 is an integral component of the core regulatory circuitry of embryonic stem cells. Genes Dev. *22*, 746–755.

Dobin, A., Davis, C.A., Schlesinger, F., Drenkow, J., Zaleski, C., Jha, S., Batut, P., Chaisson, M., and Gingeras, T.R. (2013). STAR: ultrafast universal RNA-seq aligner. Bioinformatics *29*, 15–21.

Edlund, T., and Jessell, T.M. (1999). Progression from extrinsic to intrinsic signaling in cell fate specification: a view from the nervous system. Cell *96*, 211–224.

Fang, W.Q., Chen, W.W., Fu, A.K., and Ip, N.Y. (2013). Axin directs the amplification and differentiation of intermediate progenitors in the developing cerebral cortex. Neuron *79*, 665–679.

Galceran, J., Miyashita-Lin, E.M., Devaney, E., Rubenstein, J.L., and Grosschedl, R. (2000). Hippocampus development and generation of dentate gyrus granule cells is regulated by LEF1. Development *127*, 469–482.

Gargiulo, G., Cesaroni, M., Serresi, M., de Vries, N., Hulsman, D., Bruggeman, S.W., Lancini, C., and van Lohuizen, M. (2013). In vivo RNAi screen for BMI1 targets identifies TGF-β/BMP-ER stress pathways as key regulators of neural- and malignant glioma-stem cell homeostasis. Cancer Cell *23*, 660–676.

Gaspard, N., Bouschet, T., Hourez, R., Dimidschstein, J., Naeije, G., van den Ameele, J., Espuny-Camacho, I., Herpoel, A., Passante, L., Schiffmann, S.N., et al. (2008). An intrinsic mechanism of corticogenesis from embryonic stem cells. Nature *455*, 351–357.

Gaspard, N., Bouschet, T., Herpoel, A., Naeije, G., van den Ameele, J., and Vanderhaeghen, P. (2009). Generation of cortical neurons from mouse embryonic stem cells. Nat. Protoc. *4*, 1454–1463.

Glickstein, S.B., Alexander, S., and Ross, M.E. (2007). Differences in cyclin D2 and D1 protein expression distinguish forebrain progenitor subsets. Cereb. Cortex *17*, 632–642.

Gohlke, J.M., Armant, O., Parham, F.M., Smith, M.V., Zimmer, C., Castro, D.S., Nguyen, L., Parker, J.S., Gradwohl, G., Portier, C.J., and Guillemot, F. (2008). Characterization of the proneural gene regulatory network during mouse telencephalon development. BMC Biol. *6*, 15.

Götz, M., and Huttner, W.B. (2005). The cell biology of neurogenesis. Nat. Rev. Mol. Cell Biol. *6*, 777–788.

Guillemot, F., and Hassan, B.A. (2017). Beyond proneural: emerging functions and regulations of proneural proteins. Curr. Opin. Neurobiol. *42*, 93–101.

Guillemot, F., Molnár, Z., Tarabykin, V., and Stoykova, A. (2006). Molecular mechanisms of cortical differentiation. Eur. J. Neurosci. *23*, 857–868.

Harrison-Uy, S.J., and Pleasure, S.J. (2012). Wnt signaling and forebrain development. Cold Spring Harb. Perspect. Biol. *4*, a008094.

Hayward, P., Kalmar, T., and Arias, A.M. (2008). Wnt/Notch signalling and information processing during development. Development *135*, 411–424.

Hirabayashi, Y., and Gotoh, Y. (2005). Stage-dependent fate determination of neural precursor cells in mouse forebrain. Neurosci. Res. *51*, 331–336.

Hirabayashi, Y., Itoh, Y., Tabata, H., Nakajima, K., Akiyama, T., Masuyama, N., and Gotoh, Y. (2004). The Wnt/beta-catenin pathway directs neuronal differentiation of cortical neural precursor cells. Development *131*, 2791–2801.

Imrichová, H., Hulselmans, G., Atak, Z.K., Potier, D., and Aerts, S. (2015). i-cisTarget 2015 update: generalized cis-regulatory enrichment analysis in human, mouse and fly. Nucleic Acids Res. *43*, W57–W64.

Ishitani, T., Matsumoto, K., Chitnis, A.B., and Itoh, M. (2005). Nrarp functions to modulate neural-crest-cell differentiation by regulating LEF1 protein stability. Nat. Cell Biol. *7*, 1106–1112.

Jirawatnotai, S., Hu, Y., Michowski, W., Elias, J.E., Becks, L., Bienvenu, F., Zagozdzon, A., Goswami, T., Wang, Y.E., Clark, A.B., et al. (2011). A function

for cyclin D1 in DNA repair uncovered by protein interactome analyses in human cancers. Nature *474*, 230–234.

Johnson, M.B., Wang, P.P., Atabay, K.D., Murphy, E.A., Doan, R.N., Hecht, J.L., and Walsh, C.A. (2015). Single-cell analysis reveals transcriptional heterogeneity of neural progenitors in human cortex. Nat. Neurosci. *18*, 637–646.

Kageyama, R., Ohtsuka, T., Shimojo, H., and Imayoshi, I. (2008). Dynamic Notch signaling in neural progenitor cells and a revised view of lateral inhibition. Nat. Neurosci. *11*, 1247–1251.

Kalita, A., Gupta, S., Singh, P., Surolia, A., and Banerjee, K. (2013). IGF-1 stimulated upregulation of cyclin D1 is mediated via STAT5 signaling pathway in neuronal cells. IUBMB Life *65*, 462–471.

Kang, W., Wong, L.C., Shi, S.H., and Hébert, J.M. (2009). The transition from radial glial to intermediate progenitor cell is inhibited by FGF signaling during corticogenesis. J. Neurosci. *29*, 14571–14580.

Kasper, M., Schnidar, H., Neill, G.W., Hanneder, M., Klingler, S., Blaas, L., Schmid, C., Hauser-Kronberger, C., Regl, G., Philpott, M.P., and Aberger, F. (2006). Selective modulation of Hedgehog/GLI target gene expression by epidermal growth factor signaling in human keratinocytes. Mol. Cell. Biol. *26*, 6283–6298.

Katoh, Y., and Katoh, M. (2009). Hedgehog target genes: mechanisms of carcinogenesis induced by aberrant hedgehog signaling activation. Curr. Mol. Med. *9*, 873–886.

Kent, W.J., Sugnet, C.W., Furey, T.S., Roskin, K.M., Pringle, T.H., Zahler, A.M., and Haussler, D. (2002). The human genome browser at UCSC. Genome Res. *12*, 996–1006.

Kim, C.H., Oda, T., Itoh, M., Jiang, D., Artinger, K.B., Chandrasekharappa, S.C., Driever, W., and Chitnis, A.B. (2000). Repressor activity of Headless/Tcf3 is essential for vertebrate head formation. Nature *407*, 913–916.

Kim, W.Y., Wang, X., Wu, Y., Doble, B.W., Patel, S., Woodgett, J.R., and Snider, W.D. (2009). GSK-3 is a master regulator of neural progenitor homeostasis. Nat. Neurosci. *12*, 1390–1397.

Kriegstein, A., and Alvarez-Buylla, A. (2009). The glial nature of embryonic and adult neural stem cells. Annu. Rev. Neurosci. *32*, 149–184.

Kuwahara, A., Hirabayashi, Y., Knoepfler, P.S., Taketo, M.M., Sakai, J., Kodama, T., and Gotoh, Y. (2010). Wnt signaling and its downstream target N-myc regulate basal progenitors in the developing neocortex. Development *137*, 1035–1044.

Lambot, M.A., Depasse, F., Noel, J.C., and Vanderhaeghen, P. (2005). Mapping labels in the human developing visual system and the evolution of binocular vision. J. Neurosci. *25*, 7232–7237.

Lange, C., Huttner, W.B., and Calegari, F. (2009). Cdk4/cyclinD1 overexpression in neural stem cells shortens G1, delays neurogenesis, and promotes the generation and expansion of basal progenitors. Cell Stem Cell *5*, 320–331.

Langmead, B., Trapnell, C., Pop, M., and Salzberg, S.L. (2009). Ultrafast and memory-efficient alignment of short DNA sequences to the human genome. Genome Biol. *10*, R25.

Lee, C.T., Ma, Y.L., and Lee, E.H. (2007). Serum- and glucocorticoid-inducible kinase1 enhances contextual fear memory formation through down-regulation of the expression of Hes5. J. Neurochem. *100*, 1531–1542.

Lehtinen, M.K., Zappaterra, M.W., Chen, X., Yang, Y.J., Hill, A.D., Lun, M., Maynard, T., Gonzalez, D., Kim, S., Ye, P., et al. (2011). The cerebrospinal fluid provides a proliferative niche for neural progenitor cells. Neuron *69*, 893–905.

Lien, W.H., Klezovitch, O., Fernandez, T.E., Delrow, J., and Vasioukhin, V. (2006). alphaE-catenin controls cerebral cortical size by regulating the hedgehog signaling pathway. Science *311*, 1609–1612.

Loo, L., Simon, J.M., Xing, L., McCoy, E.S., Niehaus, J.K., Guo, J., Anton, E.S., and Zylka, M.J. (2019). Single-cell transcriptomic analysis of mouse neocortical development. Nat. Commun. *10*, 134.

Lu, L., Gao, Y., Zhang, Z., Cao, Q., Zhang, X., Zou, J., and Cao, Y. (2015). Kdm2a/b lysine demethylases regulate canonical Wnt signaling by modulating the stability of nuclear β-catenin. Dev. Cell *33*, 660–674.

MacDonald, B.T., Tamai, K., and He, X. (2009). Wnt/β-catenin signaling: components, mechanisms, and diseases. Dev. Cell *17*, 9–26.

Mall, M., Kareta, M.S., Chanda, S., Ahlenius, H., Perotti, N., Zhou, B., Grieder, S.D., Ge, X., Drake, S., Euong Ang, C., et al. (2017). Myt1l safeguards neuronal identity by actively repressing many non-neuronal fates. Nature *544*, 245–249.

Mao, Y., Ge, X., Frank, C.L., Madison, J.M., Koehler, A.N., Doud, M.K., Tassa, C., Berry, E.M., Soda, T., Singh, K.K., et al. (2009). Disrupted in schizophrenia 1 regulates neuronal progenitor proliferation via modulation of GSK3beta/beta-catenin signaling. Cell *136*, 1017–1031.

Martynoga, B., Drechsel, D., and Guillemot, F. (2012). Molecular control of neurogenesis: a view from the mammalian cerebral cortex. Cold Spring Harb. Perspect. Biol. *4*, a008359.

Mateo, J.L., van den Berg, D.L.C., Haeussler, M., Drechsel, D., Gaber, Z.B., Castro, D.S., Robson, P., Lu, Q.R., Crawford, G.E., Flicek, P., et al. (2015). Characterization of the neural stem cell gene regulatory network identifies OLIG2 as a multifunctional regulator of self-renewal. Genome Res. *25*, 41–56.

McLean, C.Y., Bristor, D., Hiller, M., Clarke, S.L., Schaar, B.T., Lowe, C.B., Wenger, A.M., and Bejerano, G. (2010). GREAT improves functional interpretation of cis-regulatory regions. Nat. Biotechnol. *28*, 495–501.

Miyama, S., Takahashi, T., Nowakowski, R.S., and Caviness, V.S., Jr. (1997). A gradient in the duration of the G1 phase in the murine neocortical proliferative epithelium. Cereb. Cortex *7*, 678–689.

Munji, R.N., Choe, Y., Li, G., Siegenthaler, J.A., and Pleasure, S.J. (2011). Wnt signaling regulates neuronal differentiation of cortical intermediate progenitors. J. Neurosci. *31*, 1676–1687.

Mutch, C.A., Schulte, J.D., Olson, E., and Chenn, A. (2010). Beta-catenin signaling negatively regulates intermediate progenitor population numbers in the developing cortex. PLoS ONE *5*, e12376.

Nelson, W.J., and Nusse, R. (2004). Convergence of Wnt, beta-catenin, and cadherin pathways. Science *303*, 1483–1487.

Nilsson, E.M., Brokken, L.J., Narvi, E., Kallio, M.J., and Härkönen, P.L. (2012). Identification of fibroblast growth factor-8b target genes associated with early and late cell cycle events in breast cancer cells. Mol. Cell. Endocrinol. *358*, 104–115.

Ohtsuka, T., Shimojo, H., Matsunaga, M., Watanabe, N., Kometani, K., Minato, N., and Kageyama, R. (2011). Gene expression profiling of neural stem cells and identification of regulators of neural differentiation during cortical development. Stem Cells *29*, 1817–1828.

Phng, L.K., Potente, M., Leslie, J.D., Babbage, J., Nyqvist, D., Lobov, I., Ondr, J.K., Rao, S., Lang, R.A., Thurston, G., and Gerhardt, H. (2009). Nrarp coordinates endothelial Notch and Wnt signaling to control vessel density in angiogenesis. Dev. Cell *16*, 70–82.

Pilaz, L.J., Patti, D., Marcy, G., Ollier, E., Pfister, S., Douglas, R.J., Betizeau, M., Gautier, E., Cortay, V., Doerflinger, N., et al. (2009). Forced G1-phase reduction alters mode of division, neuron number, and laminar phenotype in the cerebral cortex. Proc. Natl. Acad. Sci. USA *106*, 21924–21929.

Rash, B.G., Lim, H.D., Breunig, J.J., and Vaccarino, F.M. (2011). FGF signaling expands embryonic cortical surface area by regulating Notch-dependent neurogenesis. J. Neurosci. *31*, 15604–15617.

Robinson, M.D., McCarthy, D.J., and Smyth, G.K. (2010). edgeR: a Bioconductor package for differential expression analysis of digital gene expression data. Bioinformatics *26*, 139–140.

Rossi, A.M., Fernandes, V.M., and Desplan, C. (2017). Timing temporal transitions during brain development. Curr. Opin. Neurobiol. *42*, 84–92.

Sakano, D., Kato, A., Parikh, N., McKnight, K., Terry, D., Stefanovic, B., and Kato, Y. (2010). BCL6 canalizes Notch-dependent transcription, excluding Mastermind-like1 from selected target genes during left-right patterning. Dev. Cell *18*, 450–462.

Sandve, G.K., Gundersen, S., Rydbeck, H., Glad, I.K., Holden, L., Holden, M., Liestøl, K., Clancy, T., Ferkingstad, E., Johansen, M., et al. (2010). The Genomic HyperBrowser: inferential genomics at the sequence level. Genome Biol. *11*, R121.

Schindelin, J., Arganda-Carreras, I., Frise, E., Kaynig, V., Longair, M., Pietzsch, T., Preibisch, S., Rueden, C., Saalfeld, S., Schmid, B., et al. (2012). Fiji: an open-source platform for biological-image analysis. Nat. Methods *9*, 676–682.

Shtutman, M., Zhurinsky, J., Simcha, I., Albanese, C., D'Amico, M., Pestell, R., and Ben-Ze'ev, A. (1999). The cyclin D1 gene is a target of the β-catenin/LEF-1 pathway. Proc. Natl. Acad. Sci. USA *96*, 5522–5527.

Shy, B.R., Wu, C.I., Khramtsova, G.F., Zhang, J.Y., Olopade, O.I., Goss, K.H., and Merrill, B.J. (2013). Regulation of Tcf7l1 DNA binding and protein stability as principal mechanisms of Wnt/β-catenin signaling. Cell Rep. *4*, 1–9.

Sur, M., and Rubenstein, J.L. (2005). Patterning and plasticity of the cerebral cortex. Science *310*, 805–810.

Tiberi, L., van den Ameele, J., Dimidschstein, J., Piccirilli, J., Gall, D., Herpoel, A., Bilheu, A., Bonnefont, J., Iacovino, M., Kyba, M., et al. (2012a). BCL6 controls neurogenesis through Sirt1-dependent epigenetic repression of selective Notch targets. Nat. Neurosci. *15*, 1627–1635.

Tiberi, L., Vanderhaeghen, P., and van den Ameele, J. (2012b). Cortical neurogenesis and morphogens: diversity of cues, sources and functions. Curr. Opin. Cell Biol. *24*, 269–276.

Tiberi, L., Bonnefont, J., van den Ameele, J., Le Bon, S.D., Herpoel, A., Bilheu, A., Baron, B.W., and Vanderhaeghen, P. (2014). A BCL6/BCOR/SIRT1 complex triggers neurogenesis and suppresses medulloblastoma by repressing Sonic Hedgehog signaling. Cancer Cell *26*, 797–812.

Tsunekawa, Y., Britto, J.M., Takahashi, M., Polleux, F., Tan, S.S., and Osumi, N. (2012). Cyclin D2 in the basal process of neural progenitors is linked to non-equivalent cell fates. EMBO J. *31*, 1879–1892.

Valenta, T., Gay, M., Steiner, S., Draganova, K., Zemke, M., Hoffmans, R., Cinelli, P., Aguet, M., Sommer, L., and Basler, K. (2011). Probing transcription-specific outputs of β-catenin in vivo. Genes Dev. *25*, 2631–2643.

Wang, L., Hou, S., and Han, Y.G. (2016). Hedgehog signaling promotes basal progenitor expansion and the growth and folding of the neocortex. Nat. Neurosci. *19*, 888–896.

Wickline, E.D., Du, Y., Stolz, D.B., Kahn, M., and Monga, S.P. (2013). γ-catenin at adherens junctions: mechanism and biologic implications in hepatocellular cancer after β-catenin knockdown. Neoplasia *15*, 421–434.

Wrobel, C.N., Mutch, C.A., Swaminathan, S., Taketo, M.M., and Chenn, A. (2007). Persistent expression of stabilized beta-catenin delays maturation of radial glial cells into intermediate progenitors. Dev. Biol. *309*, 285–297.

Wu, C.I., Hoffman, J.A., Shy, B.R., Ford, E.M., Fuchs, E., Nguyen, H., and Merrill, B.J. (2012). Function of Wnt/β-catenin in counteracting Tcf3 repression through the Tcf3-β-catenin interaction. Development *139*, 2118–2129.

Ye, B.H., Cattoretti, G., Shen, Q., Zhang, J., Hawe, N., de Waard, R., Leung, C., Nouri-Shirazi, M., Orazi, A., Chaganti, R.S., et al. (1997). The BCL-6 proto-oncogene controls germinal-centre formation and Th2-type inflammation. Nat. Genet. *16*, 161–170.

Yi, F., Pereira, L., Hoffman, J.A., Shy, B.R., Yuen, C.M., Liu, D.R., and Merrill, B.J. (2011). Opposing effects of Tcf3 and Tcf1 control Wnt stimulation of embryonic stem cell self-renewal. Nat. Cell Biol. *13*, 762–770.

Yu, Q., Sicinska, E., Geng, Y., Ahnström, M., Zagozdzon, A., Kong, Y., Gardner, H., Kiyokawa, H., Harris, L.N., Stål, O., and Sicinski, P. (2006). Requirement for CDK4 kinase function in breast cancer. Cancer Cell *9*, 23–32.

Zhang, S.J., Steijaert, M.N., Lau, D., Schütz, G., Delucinge-Vivier, C., Descombes, P., and Bading, H. (2007). Decoding NMDA receptor signaling: identification of genomic programs specifying neuronal survival and death. Neuron *53*, 549–562.

Zhang, Y., Liu, T., Meyer, C.A., Eeckhoute, J., Johnson, D.S., Bernstein, B.E., Nusbaum, C., Myers, R.M., Brown, M., Li, W., and Liu, X.S. (2008). Model-based analysis of ChIP-seq (MACS). Genome Biol. *9*, R137.

Zhang, J., Woodhead, G.J., Swaminathan, S.K., Noles, S.R., McQuinn, E.R., Pisarek, A.J., Stocker, A.M., Mutch, C.A., Funatsu, N., and Chenn, A. (2010). Cortical neural precursors inhibit their own differentiation via N-cadherin maintenance of beta-catenin signaling. Dev. Cell *18*, 472–479.

STAR★METHODS

KEY RESOURCES TABLE

REAGENT or RESOURCE	SOURCE	IDENTIFIER
Genetically Modified Organisms		
Bcl6tm2Rdf/Bcl6tm2Rdf mouse	Ye et al., 1997	MGI Cat# 3582783, RRID: MGI:3582783
Antibodies		
Chicken anti-GFP	Abcam	Cat# ab13970, RRID: AB_300798
Rabbit anti-Pax6	Covance	Cat# PRB-278P, RRID: AB_291612
Mouse anti-β3-tubulin (Tuj1)	Covance	Cat# MMS-435P, RRID: AB_2313773
Goat Sox2	Santa Cruz Biotechnology	Cat# sc-17320, RRID: AB_2286684
Mouse PCNA	Millipore	Cat# MAB424, RRID: AB_95106
Rat Phospho-Histone H3	Abcam	Cat# ab10543, RRID: AB_2295065
Rabbit Tbr2	Abcam	Cat# ab183991, RRID: AB_2721040
Rabbit Neurod2	Abcam	Cat# ab104430, RRID: AB_10975628
Alexa Fluor 488 anti-chicken	Thermo Fisher Scientific	Cat# A-11039 RRID: AB_2534096
Cyanine3 donkey anti-mouse	Jackson ImmunoResearch	Cat# 715-165-150, RRID: AB_2340813
Cyanine3 donkey anti-rabbit	Jackson ImmunoResearch	Cat# 711-165-152, RRID: AB_2307443
Rabbit IgG isotype control	Abcam	Cat# ab171870, RRID: AB_2687657
Rabbit anti-Bcl6	Santa Cruz Biotechnology	Cat# sc-858, RRID: AB_2063450
Rabbit anti-H1.4K26ac	Sigma-Aldrich	Cat# H7789, RRID: AB_1079058
Rabbit anti-H4K16ac	Millipore	Cat# 07-329, RRID: AB_310525
Rabbit anti-Sirt1	Millipore	Cat# 07-131, RRID: AB_10067921
Rabbit anti-Tcf7l1	Prof. Brad Merrill	N/A
Chemicals, Peptides, and Recombinant Proteins		
CHIR 99021	Tocris	Cat# 4423
Cyclopamine	Calbiochem	Cat# 239803
Doxycycline hydrochloride	Sigma-Aldrich	Cat# D3447
ESGRO Recombinant LIF	Merck	Cat# ESG1107
N-2 Supplement	Thermo Fisher Scientific	Cat# 17502048
Critical Commercial Assays		
HiSeq PE Cluster Kit v4	Illumina	Cat# PE-401-4001
RNeasy mini kit	QIAGEN	Cat# 74104
TruSeq SBS Kit v3-HS	Illumina	Cat# FC-401-3002
TruSeq stranded mRNA library prep	Illumina	Cat# RS-122-2101
DIG RNA labeling kit	Roche	Cat# 11175025910
qPCR Primers		
Oligonucleotides	Eurogentec	See Table S4
Experimental Models: Cell Lines		
A2 lox.Cre Bcl6 ES cells	Tiberi et al., 2012a	N/A
Experimental Models: Organisms/Strains		
Mouse: ICR (CD1)	Janvier labs	Strain code 022
Deposited Data		
ChIP-seq	This paper	GEO: GSE132964
RNA-seq	This paper	GEO: GSE133031

(*Continued on next page*)

Continued

REAGENT or RESOURCE	SOURCE	IDENTIFIER
Software and Algorithms		
Bowtie	Langmead et al., 2009	https://github.com/BenLangmead/bowtie
EdgeR 3.20.1	Robinson et al., 2010	https://bioconductor.org/packages/release/bioc/html/edgeR.html
Fiji/ImageJ 1.49b	Schindelin et al., 2012	https://fiji.sc/
Genomic HyperBrowser	Sandve et al., 2010	https://hyperbrowser.uio.no/hb/
GOrilla		http://cbl-gorilla.cs.technion.ac.il
GREAT 3.0	McLean et al., 2010	http://great.stanford.edu/public/html/
HTSeq 0.9.1	Anders et al., 2015	https://github.com/simon-anders/htseq
i-cisTarget	Imrichová et al., 2015	https://gbiomed.kuleuven.be/apps/lcb/i-cisTarget/
MACS	Zhang et al., 2008	https://github.com/taoliu/MACS/
STAR 2.5.3a	Dobin et al., 2013	https://github.com/alexdobin/STAR
UCSC Genome Browser	Kent et al., 2002	https://genome.ucsc.edu
ZEN Black microscope software	Zeiss	N/A
Other		
Axioplan2 fluorescent microscope	Zeiss	N/A
LSM780 confocal microscope	Zeiss	N/A

LEAD CONTACT AND MATERIALS AVAILABILITY

Further information and requests for resources and reagents should be directed to, and will be fulfilled without restriction by, the Lead Contact Pierre Vanderhaeghen (pierre.vanderhaeghen@kuleuven.vib.be).

EXPERIMENTAL MODEL AND SUBJECT DETAILS

Animals

All mouse experiments were performed with the approval of the Université Libre de Bruxelles Committee for animal welfare. Animals were housed under standard conditions (12 h light:12 h dark cycles) with food and water *ad libitum*. For in utero electroporation experiments, timed-pregnant mice were obtained by mating adult RjOrl:SWISS CD1 mice (Janvier, France). The plug date was defined as embryonic day E0.5. For experiments using *Bcl6*$^{-/-}$ mice, we mated *Bcl6*$^{+/-}$ mice (mixed C57BL/6 and CD1 background), in which the null allele lacked exons 4–10 (Ye et al., 1997).

METHOD DETAILS

In Utero Electroporation

Timed-pregnant mice were anesthetized with a ketamine/xylazine mixture at E13.5. Each uterus was cautiously exposed under sterile conditions. Fast-green (Sigma)-labeled plasmid solutions were prepared using either 1 μg/μL or 0.5 μg/μL of appropriate DNA combinations for gain of function experiments or knockdown experiments, respectively. DNA solutions were injected into the lateral ventricles of the embryos using a heat-pulled glass capillary (1.0 OD x 0.78 × 100 L mm; Harvard Apparatus) prepared with a heat micropipette puller (heat: 580, pull: 100, velocity: 170, time: 120, pressure: 500; Sutter Instrument P-87). Electroporation was performed using tweezers electrodes (Nepa Gene CUY650P5) connected to a BTX830 electroporator (5 pulses of 30 V for 100 ms with an interval of 1 s). Embryos were placed back into the abdominal cavity, and mice were sutured and placed on a heating plate until recovery.

Mouse ES cells and cortical differentiation

The A2 lox.Cre Bcl6 cell lines, tetracyclin-inducible Bcl6 ICE (A2lox.Cre) mouse Embryonic Stem Cells (Tiberi et al., 2012a), were routinely propagated on irradiated mouse embryonic fibroblasts in DMEM (Invitrogen) supplemented with 15% ESC-certified fetal bovine serum (vol/vol, Invitrogen), 0.1 mM non-essential amino acids (Invitrogen), 1 mM sodium pyruvate (Invitrogen), 0.1 mM β-mercaptoethanol (Sigma), 50 U.ml^{-1} penicillin/ streptomycin and 10^3 U.ml^{-1} mouse Leukemia Inhibitor Factor (ESGRO). Results were obtained using three independent clones.

For differentiation, A2 lox.Cre Bcl6 mouse ESCs were plated at low density (20 × 10^3 ml^{-1}) on gelatin-coated coverslips and cultured as previously described (Gaspard et al., 2009). Briefly, on day 0 of the differentiation, the ES medium was changed to

DDM medium. At day 2, DDM was supplemented with cyclopamine (400 ng/mL, Calbiochem) and the medium was replenished every 2 days. After 10 days, medium was switched back to DDM. Doxycline treatment (1 $\mu g.ml^{-1}$) for Bcl6 induction or DMSO (1:1000, control) was applied for 6,12 or 24 h at day 12. CHIR99021 (4 μM, Tocris) needed to be applied for 48h, i.e., from day 10, to effectively impact Wnt target genes.

Plasmids

For *in situ* hybridization, the *Ccnd1* coding sequences (888 bp) and the *Ccnd2* 5′UTR+coding sequence (1145 bp) were amplified by PCR from ESC-derived cortical progenitor cDNA, and the sequences verified and cloned into pGEMT plasmid (Promega). The *Axin2* plasmid was a kind gift from Dr I. Garcia (ULB) and the *Lmo4* plasmid was a kind gift from Prof. J.L.R. Rubenstein (UCSF), who received it from Prof. G.N. Gill (UCSD). For in utero electroporations, the *Bcl6* coding sequence was amplified by PCR from cDNA and cloned into p*CAG*-IRES-*GFP* (pCIG). The p*CAG*-Δ90*Ctnnb1* plasmid (N-terminal deletion lacking GSK3-dependent S^{33}, S^{37} and T^{41} phosphorylation sites) was obtained from Addgene (plasmid #26645). The p*CAG-Ccnd1* and p*EF1α-Tcf7l1* plasmids were kind gifts from Dr C. Dehay and Prof. R. Kageyama, respectively. The shRNA plasmids were cloned downstream of the *U6* promoter into the pSilencer2.1-CAG-Venus (pSCV2)-plasmid as previously described (Tiberi et al., 2012a) with the exception of the *Ctnnb1* shRNA plasmid (pLKO.1-puro vector, Sigma). Target sequences were 5′-ACTACCGTTGTTATAGGTG-3′ (Control; Tiberi et al., 2012a), 5′-TGATGTTCTTCTCAACCTTAA-3′ (*Bcl6*; Tiberi et al., 2012a; Zhang et al., 2007), 5′-CCCAAGCCTTAGTAAACAT AA-3′ (*Ctnnb1*; Mao et al., 2009), 5′- AGCCTGCACCAGGACTAC-3′ (*Hes5*; (Lee et al., 2007), 5′-CCACAGATGTGAAGTTCATTT-3′ (*Ccnd1*; Jirawatnotai et al., 2011; Yu et al., 2006), 5′-CGACTTCAAGTTTGCCATGTA-3′ (*Ccnd2*; Gargiulo et al., 2013) and were previously validated in the corresponding references.

Immunofluorescence

Embryos were fixed by transcardiac perfusion with freshly-prepared 4% paraformaldehyde (Sigma). Brains were dissected, and 100 mm sections were prepared using a Leica VT1000S vibrosector. Slices were transferred into PBS with 0.5 μg/mL sodium azide (Sigma), then blocked with PBS supplemented with 3% horse serum (Invitrogen) and 0.3% Triton X-100 (Sigma) during 1 h, and incubated overnight at 4°C with the following primary antibodies: chicken GFP (Abcam, 1:2,000), rabbit Pax6 (Covance, 1:1000), Sox2 (Santa Cruz Biotechnology, 1:500), PCNA (Millipore, 1:200), phospho-Histone H3 (Abcam, 1:100), Tbr2 (Abcam, 1:500), Neurod2 (Abcam, 1:500), or mouse β3-tubulin (Tuj1 epitope, Covance, 1:1000). After three washes with PBS/0.1% Triton X-100, slices were incubated in PBS for 1 h at room temperature and incubated 2 h at room temperature with the appropriated Alexa 488 (1:1,000, Molecular Probes), Cyanine 3 or Cyanine 5 (1:400, Jackson ImmunoResearch) secondary antibodies. Sections were again washed three times with PBS/0.1% Triton X-100, stained with Hoechst (bisBenzimide H 33258, Sigma) for 5 min and washed twice in PBS. The sections were next mounted on a Superfrost slide (Thermo Scientific) and dried using a brush before adding Glycergel mounting medium (Dako). Imaging was performed using a Zeiss LSM780 confocal microscope controlled by the Zen Black software (Zeiss).

Transcriptome analyses

Total mRNA from four independent samples from ESc-derived cortical differentiations (day 12 ± doxycycline) was extracted using the QIAGEN RNeasy mini kit according to the manufacturer's recommendations. Following RNA quality control assessed on a Bioanalyzer 2100 (Agilent technologies), the indexed cDNA libraries were prepared using the TruSeq stranded mRNA Library Preparation kit (Illumina) following manufacturer's recommendations. The multiplexed libraries (18 pM) were loaded on flow cells and sequences were produced using a HiSeq PE Cluster Kit v4 and TruSeq SBS Kit v3-HS from a Hiseq 1500 (Illumina). Approximately 20 million of paired-end reads per sample were mapped against the mouse reference genome (GRCm38.p4/mm10) using STAR 2.5.3a software (Dobin et al., 2013) to generate read alignments for each sample. Annotations Mus_musculus.GRCm38.87.gtf were obtained from ftp.Ensembl.org. After transcript assembling, gene level counts were obtained using HTSeq 0.9.1 (Anders et al., 2015). EdgeR 3.20.1 (Robinson et al., 2010) was then used to calculate the level of differential gene expression. Gene Ontology analyses of biological processes were performed using the GOrilla application (http://cbl-gorilla.cs.technion.ac.il).

RT-qPCR

Reverse transcription of mature mRNAs was done with the Superscript II kit (Invitrogen) using the manufacturer's protocol for oligo dTs. Quantitative PCR (qPCR) was performed in duplicate using Power Sybr Green Mix (Applied Biosystems) and a 7500 Real-Time PCR System (Applied Biosystems). Results are presented as linearized Ct values normalized to the housekeeping gene *Tbp* ($2^{-\Delta Ct}$) and the primers are listed in the Table S4.

In situ RNA hybridization

Whole-mount *in situ* hybridization as well as on coronal and sagittal cryosections was performed using digoxigenin-labeled RNA probes (DIG RNA labeling kit, Roche) and alkaline phosphatase revelation (NBT/BCIP kit #SK-5400; Vector) as previously described (Lambot et al., 2005). The above-mentioned plasmids were linearized and reverse-transcribed to generate the anti-sense probes. Sense probes were used as a negative control for each gene tested and revealed no specific staining (data not shown). Images were acquired with a Zeiss Axioplan 2 microscope and a Spot RT3 camera using the Spot 5.2 software. For quantifications, littermate

embryos were compared using 3 animals/genotype from 3 different litters for *Axin2* and *Ccnd2* or 6 embryos/genotype from 4 different litters (*Ccnd1*). Quantifications of gray densities were done on comparable levels of the dorsal primordium of the frontal cortex using ImageJ software (Schindelin et al., 2012).

Chromatin Immunoprecipitation

A2 lox.Cre Bcl6 cells and E12.5 *Bcl6* WT and KO telencephalons were fixed with 1% formaldehyde in phosphate-buffered saline and then lysed, sonicated, and immunoprecipitated as described previously (Castro et al., 2011). Immunoprecipitations were performed using IgG isotype control (ab171870, Abcam), Bcl6 (sc-858, Santa Cruz Biotechnology), H1.4K26ac (H7789, Sigma-Aldrich), H4K16ac (07-329, Millipore), Sirt1 (07-131, Millipore), and Tcf7l1 (kind gift from Prof. Brad Merrill) rabbit antibodies and 50/50 mixed protein A and protein G magnetic Dynabeads (ThermoFisher Scientific). Primers used for ChIP-qPCR were designed to surround the predicted Bcl6 matrices present in the significant peaks of the ChIP-seq screen and are listed in the Table S4.

ChIP-seq

Following chromatin immunoprecipitation using A2 lox.Cre Bcl6 cells (differentiation day 12, 24h Bcl6 induction using 1 $\mu g.ml^{-1}$ Doxycline treatment) as described above, ChIP libraries were prepared according to the standard Illumina ChIP-seq protocol and were sequenced with the Genome Analyzer IIx (Illumina) as previously described (Mateo et al., 2015). Reads from three independent ChIP-seq experiments were pooled and aligned to mm10 mouse genome assembly using Bowtie (Langmead et al., 2009). Peaks were then called using MACS (Zhang et al., 2008) with standard parameters with default cutoff p value < 10e-5. Target genes associated with peaks were identified by GREAT version 3.0 (McLean et al., 2010). ChIP-seq dataset for the Bcl6-predicted target genes were visualized using the UCSC Genome Browser (Kent et al., 2002). Search for an enrichment of Bcl6 matrices in the MACS-called ChIP peaks was performed using i-cisTarget (Imrichová et al., 2015) using a promoter-only database.

QUANTIFICATION AND STATISTICAL ANALYSIS

Results are shown as mean ± standard error (SEM) of at least three biologically independent experiments. Student's unpaired t test was used for two group comparisons. Analyses of multiple groups were performed by a one-way or two-way analysis of variance (ANOVA) - as indicated in figure legends - followed by post hoc multiple comparisons using Tukey's test. Hypothesis testing for overlap analysis was performed using the Genomic HyperBrowser (https://hyperbrowser.uio.no/hb/; Sandve et al., 2010). For all tests, a p value inferior to 0.05 was taken as statistically significant.

DATA AND CODE AVAILABILITY

RNA-seq raw data are shown on Table S5 and the complete dataset is available at GEO repository (GEO: GSE133031). The ChIP-seq dataset is available at GEO repository (GEO: GSE132964).

Neuron, Volume *103*

Supplemental Information

Cortical Neurogenesis Requires Bcl6-Mediated Transcriptional Repression of Multiple Self-Renewal-Promoting Extrinsic Pathways

Jerome Bonnefont, Luca Tiberi, Jelle van den Ameele, Delphine Potier, Zachary B. Gaber, Xionghui Lin, Angéline Bilheu, Adèle Herpoel, Fausto D. Velez Bravo, François Guillemot, Stein Aerts, and Pierre Vanderhaeghen

Supplementary Figure S1

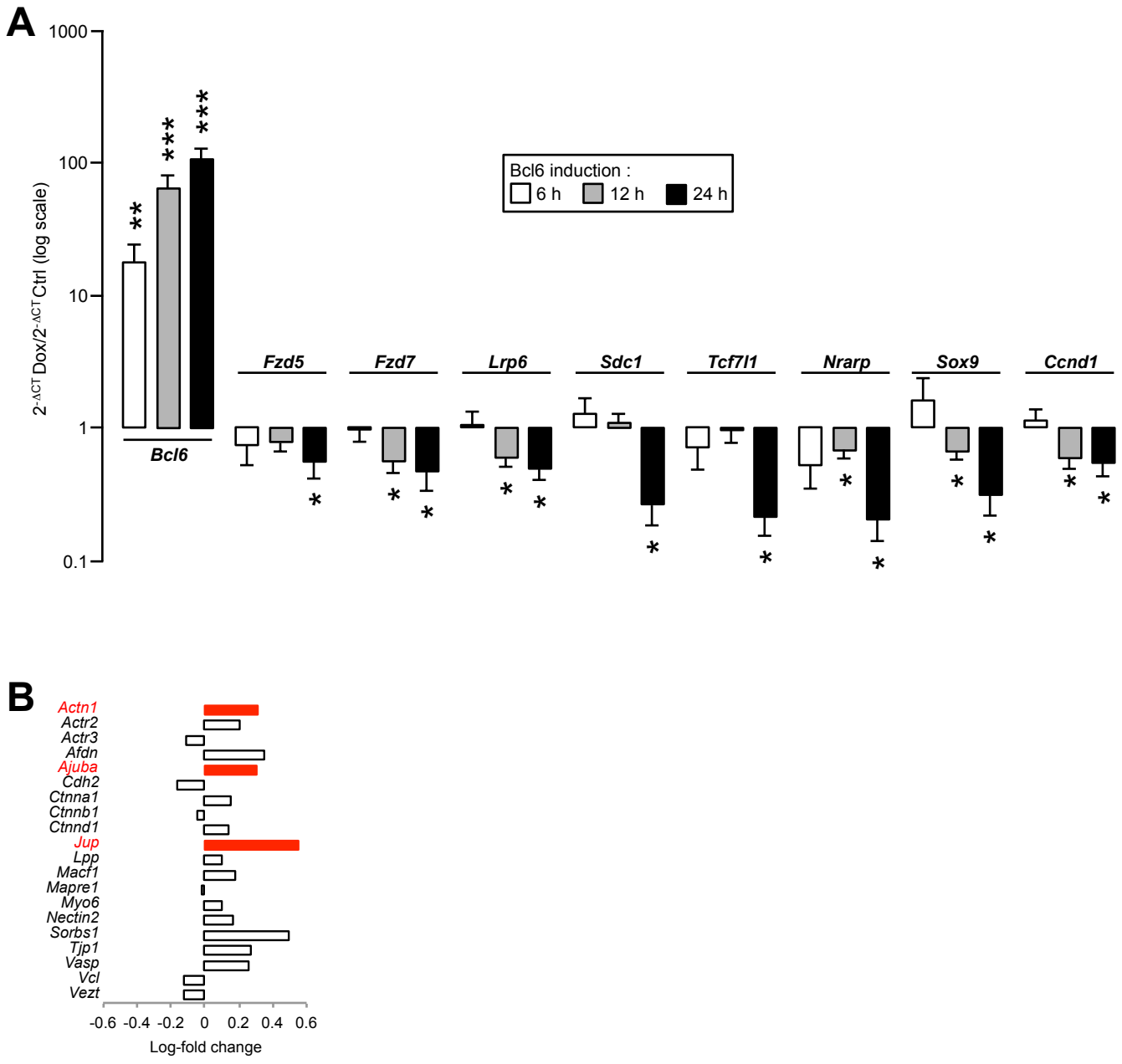

Supplementary Figure S1. Related to Figure 1. (A) Bcl6-mediated down-regulation of Wnt-related genes occurs before changes in cell identity markers. RT-qPCR analysis of *Bcl6* and additional Wnt-related genes in day 12 *in vitro* cortical progenitor cells treated with DMSO (Control) or doxycycline for 6, 12 or 24h. Data are presented as mean + s.e.m. of Dox/Ctrl absolute levels (*n* = 7-9 (6h), 27-30 (12h), and 9 (24h) from at least 3 independent differentiations for each group). * *P*<0.05, ** *P*<0.01, *** *P*<0.001. **(B) Bcl6 impact on adherens junction-related genes.** Histograms representing the log-fold change of the main genes involved in the formation/function of catenin-based adherens junctions following induction of Bcl6 expression in *in vitro* ES cell-derived cortical progenitors. Significantly overexpressed genes are indicated in red.

Supplementary Figure 2

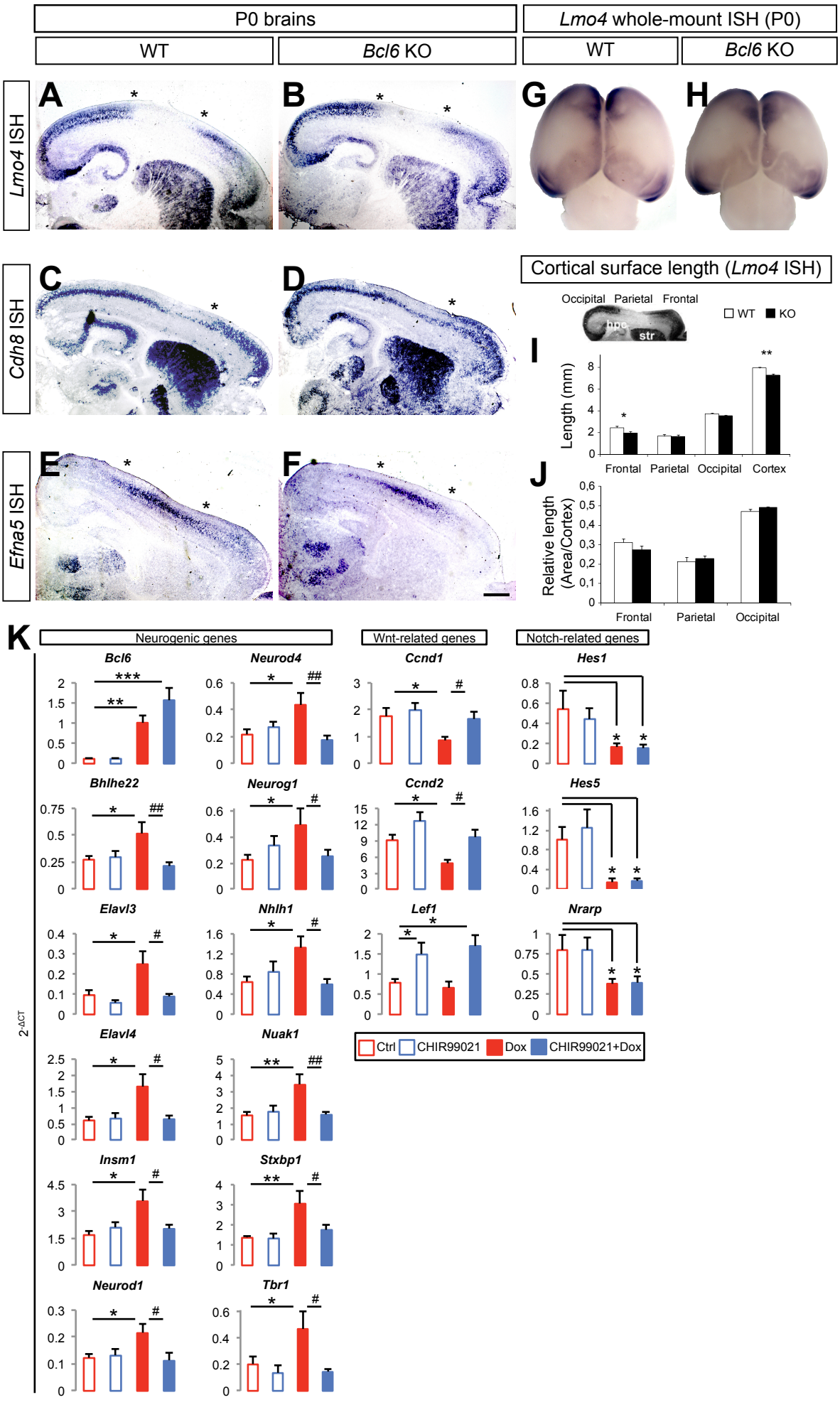

Supplementary Figure S2. Related to Figure 2. (A-J) Bcl6 is not required for proper establishment of primary cortical areas. (A-F) *In situ* hybridization on sagittal sections of wild-type and *Bcl6* KO brains at P0 with antisense probes for *Lmo4* (A-B), *Cdh8* (C-D) and *Efna5* (E-F). Scale bar, 200 μm. (G-H) Whole-mount *in situ* hybridization wild-type and *Bcl6* KO brains at P0 with an antisense probe for *Lmo4*. (I-J) Quantification of the absolute (I) or relative (J) lengths of the cortical surface of the frontal, parietal and occipital domains of wild-type and *Bcl6* KO cortices at P0 as delineated by borders of *Lmo4 in situ* hybridization on comparable sagittal sections (depicted in the scheme; hpc, hippocampus; str, striatum). Data are presented as mean + s.e.m. (n=5 (WT) and 6 (*Bcl6* KO) sections from 3 brains each). * $P<0.05$, ** $P<0.01$. **(K) Bcl6-mediated up-regulation of neurogenic genes is prevented by β-catenin overactivation using the GSK3 inhibitor, CHIR99021.** RT-qPCR analysis of neurogenic markers, Wnt targets and Notch targets in cortical progenitors derived from *Bcl6* A2 lox.Cre mouse ES cells (differentiation day 12) treated with DMSO (Control), CHIR99021, doxycycline and CHIR99021+doxycycline. Data are presented as mean + s.e.m. of absolute levels (n = 9 differentiations). * $P<0.05$, ** $P<0.01$, *** $P<0.001$ Bcl6 overexpression (doxycycline) vs. control and $^{\#}$ $P<0.05$, $^{\#\#}$ $P<0.01$ CHIR+Dox vs. Bcl6 overexpression (doxycycline).

Supplementary Figure S3

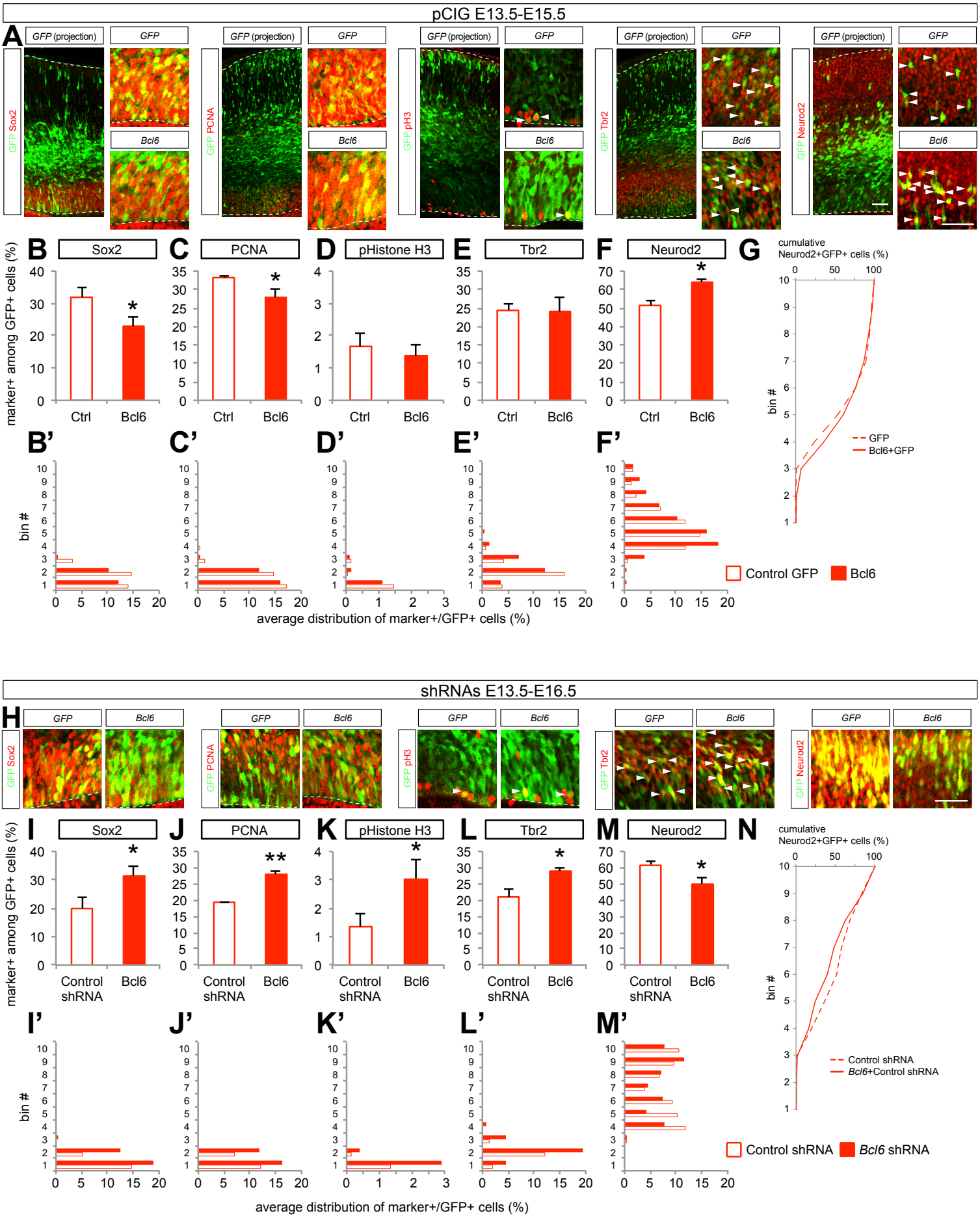

Supplementary Figure S3. Related to Figures 2 and 3. Characterization of Bcl6 neurogenic activity following its overexpression or knockdown using *in utero* electroporation. (A) Confocal images of immunofluorescence on coronal sections of E15.5 brains for cell fate and proliferation markers following *in utero* electroporation of control pCIG or pCIG-*Bcl6* at E13.5 using maximal intensity projection of Control z-stacks (whole cortical thickness) or a single z plan. Dashed lines represent the apical margin of the ventricular zone. Arrowheads point at double positive cells. Scale bars represent 50 μm. (B-F) Histograms show the percentage of Sox2+, PCNA+, pH3+, Tbr2+ and Neurod2+ cells among the GFP+ cells. Data are presented as mean + s.e.m. * $P<0.05$. (B'-F') Bin analysis of the average distribution of the markers+GFP+ cell populations quantified in B-F. (G) Assessment of neuronal migration behavior using bin analysis of cumulative Neurod2+GFP+ cells. (H) Single confocal z plan of immunofluorescence on coronal sections of E16.5 brains for cell fate and proliferation markers following *in utero* electroporation of scramble (control) or scramble+*Bcl6* shRNAs at E13.5. Dashed lines represent the apical margin of the ventricular zone. Arrowheads point at double positive cells. Scale bar, 50 μm. (I-M) Histograms show the percentage of Sox2+, PCNA+, pH3+, Tbr2+ and Neurod2+ cells among the GFP+ cells. Data are presented as mean + s.e.m. * $P<0.05$, ** $P<0.01$. (I'-M') Bin analysis of the average distribution of the markers+GFP+ cell populations quantified in I-M. (N) Assessment of neuronal migration behavior using bin analysis of cumulative Neurod2+GFP+ cells.

Supplementary Figure S4

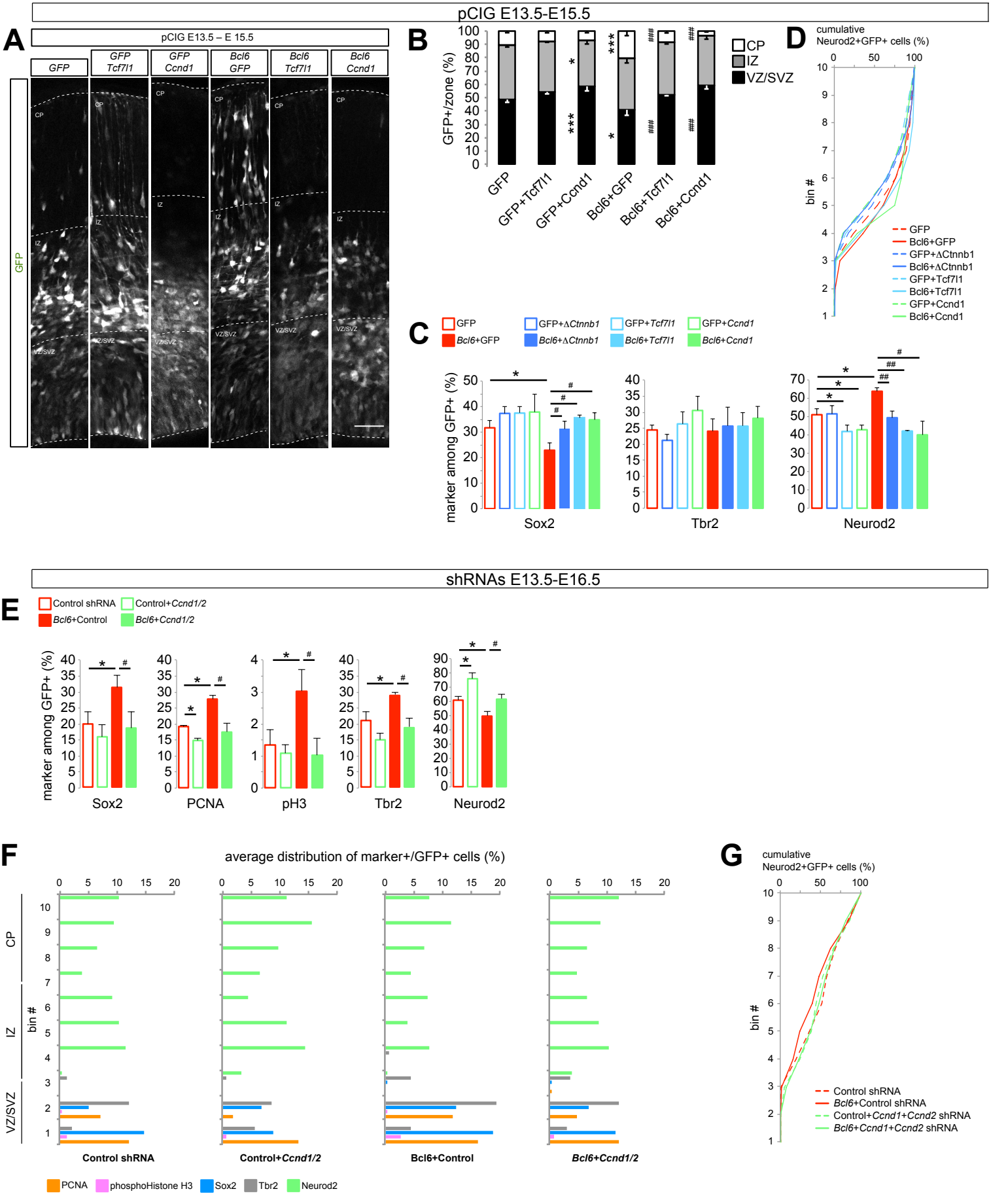

Supplementary Figure S4. Related to Figures 2 and 3. (A-D) Bcl6-elicited neurogenesis is blocked *in vivo* by β-Catenin, Tcf7l1 and Ccnd1 overexpression. . *In utero* electroporation of pCIG, pCIG+pCAG-*Δ(1-90)Ctnnb1*, pCIG+pEF1α-*Tcf7l1*, pCIG+pCAG-*Ccnd1*, pCIG-*Bcl6*+pCIG, pCIG-*Bcl6*+pCAG-Δ(1-90)*Ctnnb1*, pCIG-*Bcl6*+ pEF1α-*Tcf7l1*, or pCIG-*Bcl6*+pCAG-*Ccnd1* at E13.5. immunofluorescence was performed on coronal sections of E15.5 brains. (A) Representative images of Hoechst and GFP immunofluorescence performed on coronal sections of E15.5 brains. Dashed lines mark the basal and apical margins of the ventricular + subventricular zone (VZ+SVZ), intermediate zone (IZ) and cortical plate (CP). Scale bar, 50 μm. (B) Histograms show the percentage of GFP+ cells in VZ+SVZ, IZ and CP. Data are presented as mean + s.e.m. * P<0.05, ** P<0.01, *** P<0.001 vs. pCIG and ### P<0.001 vs. pCIG-*Bcl6*+pCIG. (C) Histograms show the percentage of Sox2+, Tbr2+ and Neurod2+ cells among the GFP+ cells. Data are presented as mean + s.e.m. * P<0.05 vs. pCIG+pCIG and # P<0.05, ## P<0.01 vs. pCIG-*Bcl6*+pCIG. (D) Assessment of neuronal migration behavior using bin analysis of cumulative Neurod2+GFP+ cells. Note that the quantifications in (C,D) for the GFP and Bcl6 groups are similar to those presented on Supplementary Figure S3B,E,F,G as all the conditions were performed simultaneously to compare phenotypes in littermate embryos. **(E-G) *Bcl6* knockdown is rescued *in vivo* by *Ccnd1* and *Ccnd2* shRNAs.** *In utero* electroporation of scramble (control), scramble+*Ccnd1*+*Ccnd2*, *Bcl6*+scramble and *Bcl6*+*Ccnd1*+*Ccnd2* shRNAs at E13.5. (E) Histograms show the percentage of Sox2+, PCNA+, phosphoHistone H3+, Tbr2+ and Neurod2+ cells among the GFP+ cells. * P<0.05 vs. Control and # P<0.05 vs. Bcl6+scramble shRNAs. Data are presented as mean + s.e.m. (F) Bin analysis of the average distribution of the markers+GFP+ cell populations quantified in A. (G) Assessment of neuronal migration behavior using bin analysis of cumulative Neurod2+GFP+ cells. Note that the quantifications for the control and Bcl6+scramble groups are similar to those presented on Supplementary Figure S3I-N as all the conditions were performed simultaneously to compare phenotypes in littermate embryos.

Supplementary Figure S5

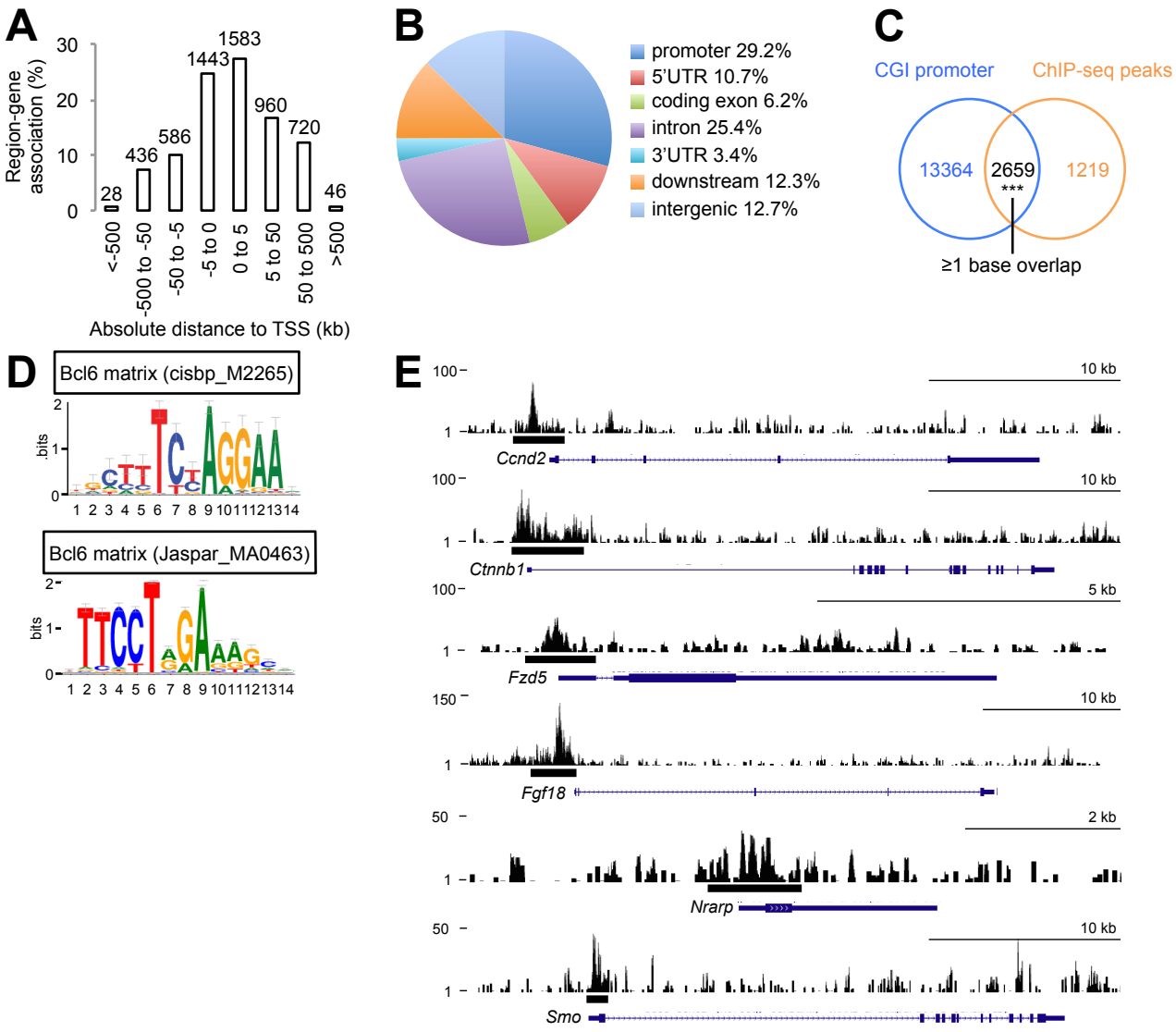

Supplementary Figure S5. Related to Figure 4. ChIP-seq analysis following Bcl6 induction in cortical progenitors derived from *Bcl6* A2 lox.Cre mouse ES cells (differentiation day 12, 24h Dox treatment). (A) Absolute distance of significant Bcl6-bound sequences to gene transcription starting sites. Numbers of region-gene associations are indicated on the histograms. (B) Pie chart localization of the significant Bcl6-bound sequences in the mouse genome. (C) Venn diagram of the overlap between the total number of CpG island promoters and the MACS-called peaks. *** *P*=9.999e-05 using a hypothesis testing for overlap analysis. (D) Significantly enriched Bcl6 matrices from the MACS-called peaks using i-cisTarget on a promoter-only database. Normalized Enrichment Score (NES) = 3.64 for the Bcl6 matrix Cisbp_M2265 and NES = 3.55 for the Bcl6 matrix Jaspar_MA0463. (E) Examples of profiles for Bcl6-predicted target genes related to Wnt, Notch, SHH, and FGF signaling. Black bars indicate MACS-called peaks and RefSeq genes from mm10 mouse genome assembly (https://genome.ucsc.edu) are represented in blue using 5' to 3' orientation.

Supplementary Figure S6

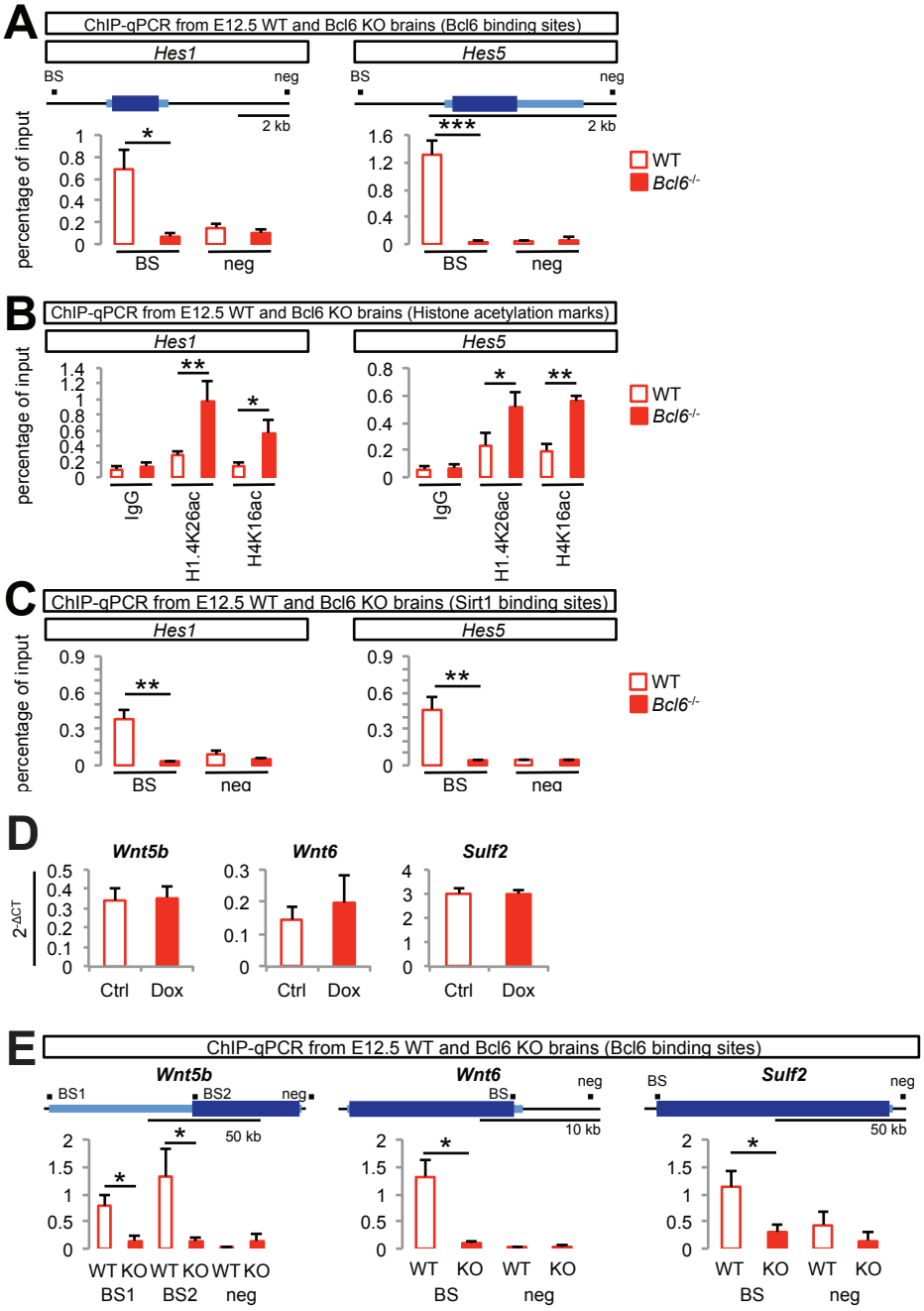

Supplementary Figure S6. Related to Figures 4 and 5. (A-C) Bcl6 binds to Notch targets, *Hes1* and *Hes5*, leading to chromatin remodeling. (A) ChIP-qPCR of Bcl6-binding sites on regulatory regions of Notch target genes, *Hes1* and *Hes5*, and negative control sites in E12.5 wild-type and *Bcl6*-/- telencephalon. Data are presented as mean + s.e.m. of input enrichment (n = 4). * $P<0.05$ and *** $P<0.001$. (B) ChIP-qPCR of histone marks H1.4K26ac and H4K16ac on Bcl6 binding sites on regulatory regions of *Hes1* and *Hes5* genes in E12.5 wild-type and *Bcl6*-/- telencephalon. Data are presented as mean + s.e.m. of input enrichment (n = 4). * $P<0.05$ and ** $P<0.01$. (C) ChIP-qPCR of Sirt1 on Bcl6 binding sites on regulatory regions of *Hes1* and *Hes5* genes in E12.5 wild-type and *Bcl6*-/- telencephalon. Data are presented as mean + s.e.m. of input enrichment (n = 4). ** $P<0.01$. **(D-E) Bcl6 also binds to some Wnt-related genes without inducing detectable transcriptional changes.** (A) RT-qPCR analysis of Wnt-related genes from DMSO- and doxycycline-treated Bcl6 A2 lox.Cre cells at day 12 of differentiation. Data are presented as mean + s.e.m. of absolute levels (n = 21 from 8 differentiations). (B) ChIP-qPCR validation of screened Bcl6-binding sites on regulatory regions and negative control sites of non-transcriptionally altered Wnt-related genes in E12.5 wild-type and *Bcl6*-/- telencephalon using a Bcl6 antibody. Data are presented as mean + s.e.m. of input enrichment (n = 4). * $P<0.05$.

Supplementary Figure S7

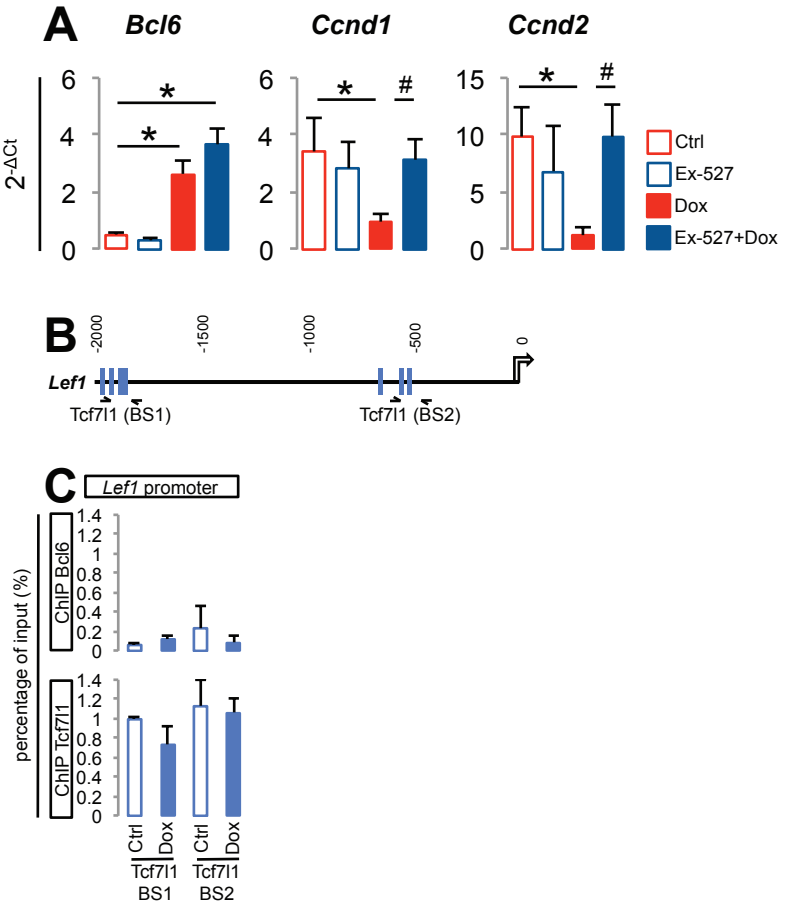

Supplementary Figure S7. Related to Figure 6. (A) Bcl6-elicited *Ccnd1/2* down-regulation is blocked by the Sirt1 inhibitor Ex-527. RT-qPCR analysis of the Bcl6 targets *Ctnnb1* and *Ccnd2* in day 12 *in vitro* ES cell-derived cortical progenitor cells (differentiation day 12, treated with DMSO (Control) or doxycycline ± Ex-527 for 24h). Data are presented as mean + s.e.m. of absolute levels (*n* = 12-18 from at least 3 independent differentiations). * $P<0.05$ vs. Control and # $P<0.05$ vs. Dox. **(B-C) Control ChIP-qPCRs of *in vitro* Tcf7l1 binding to the 5' regulatory region of the Wnt target gene *Lef1* upon Bcl6 induction.** (B) Schematic representation of the genomic region 2 kb upstream from *Lef1* transcription starting site showing putative Tcf7l1 binding sites as predicted by the Jaspar software (http://jaspar.genereg.net). The arrows represent the amplified regions by qPCR used to measure the enrichment following ChIP. (C) ChIP-qPCR analysis of the Tcf7l1 binding sites on the *Lef1* regulatory region in cortical progenitors derived from *Bcl6* A2 lox.Cre mouse ES cells (differentiation day 12, 24h DMSO (Ctrl) or Dox treatment) using Bcl6 and Tcf7l1 antibodies. Data are presented as mean + s.e.m. of input enrichment (n = 3 differentiations).